Transcriptomic analyses reveal prenatal stress promotes late-onset neural stem cell proliferation in adult male offspring

Z. Wang[1,*], L.Q. Zhou[1,*,†], C.M. Lee[2, *, ψ], J.Y. Shi[1], L. Liu[2], X.J. Yang[1], Y.X. Deng[1], J.P. Liu[3], J.B. Wang[3], W.M. Zhu[1,3], Y.E. Sun[1,3,†], and Q. Lin[1,2,†]

[1] Shanghai Institute of Stem Cell Research and Clinical Translation, Shanghai East Hospital, School of Medicine, Tongji University, Shanghai, China.

[2] Department of Psychiatry and Behavioral Sciences, Intellectual Development and Disabilities Research Center, University of California, Los Angeles, CA 90095

[3] Stem Cell Translational Research Center, Tongji Hospital, School of Medicine, Tongji University, Shanghai, China.

[*] Equal contribution

[ψ] Current address: Des Moines University, 3200 Grand Ave. Des Moines, IA 50312

[†] To whom correspondence may be addressed. Q.L. qlin@g.ucla.edu, Y.E.S. yievesun@gmail.com, or jason_li_zhou@126.com

Abstract

Perturbations during critical time windows during embryonic development can lead to adverse functional consequences that manifest later in life. Here, we report that prenatal maternal stress (PNS) during the peak of embryonic neurogenesis (E14-delivery) dramatically increased numbers of proliferating neural stem/progenitor cells (NSC/NPCs) in the ependymal-subventricular zone (E-SVZ) and neuroblasts (NBs) in the rostral migratory stream and newborn neurons in the olfactory bulb (OB) of male mouse offspring without causing significant cell death or a deficit in cell migration to the OB. Mechanistically, bulk and single-nucleus transcriptomic analyses showed that PNS affected gene regulatory networks controlling cell cycle progression and stem cell maintenance, maturation of neural circuits, and gliogenesis in prenatally stressed (STR) offspring. More specifically, we found that prenatal exposure to mild maternal restraint-stress sustained MAPK (ERK) activity in the E-SVZ and thus prolonged NSC/NPC/NB proliferation in stressed brains. Moreover, we found PNS disorganized the cytoarchitecture of the glomerular layer of the OB, which may directly relate to the deficit in discriminating different social orders in stressed offspring. Compared to STR males, their female littermates showed less change in the number of proliferating cells in the E-SVZ.

Introduction

In humans and model animals, environmental disturbances during the critical period have been shown to cause neural morphological, neurobiological, and behavioral deficits [1-11]. Since the evidence of cell mitosis in the SVZ of adult rats was published over 100 years ago [12], it has now been widely accepted that adult neurogenesis occurs in mammals [13-17]. Numerous studies have reported that the ependymal-subventricular zone (E-SVZ) and the dentate gyrus (DG) are the brain regions that harbor NSC/NPCs to give rise to neurons and glial cells throughout life [14, 15, 18-22]. Mechanistically, epidermal growth factor (EGF) and vascular endothelial growth factor (VEGF) are two key extrinsic factors to activate dormant/quiescent neural stem cell and neural progenitor cell proliferation in the E-SVZ of the ventricles in mouse brain [14, 19]. MAPK (a.k.a. extracellular signal-regulated kinase (ERK)) cascade, as a major transducer of growth factors like EGF and VEGF, plays a vital role in mediating their intracellular signaling [23, 24]. MAPK(ERK) has a TxY motif in its activation domain, which requires dual phosphorylation by upstream MAPK kinases (e.g., MAP2K1/2 (MEK1/2)) for catalytic activation. MAPK3 and 1 (ERK1/2) have been shown to interact with wide-range signaling pathways, such as EGF/FGF/VEGF, WNT, BMP/TGFB, Estrogen, and SHH [25-29] to regulate cell proliferation and to facilitate epithelial-mesenchymal transition (EMT) in cancer cells [30, 31].

Although tremendous progress has been made to understand the long-lasting effects of PNS on brain development, little is known about the molecular programs that govern adult NSC/NPC proliferation and neurogenesis in response to prenatal stimuli. In the current study, we found that mild, prenatal maternal restraint stress increased the numbers of $BrdU^+$ and $MKI67^+$ proliferating cells in the E-SVZ and the rostral migratory

stream (RMS) and the number of BrdU$^+$/RBFOX3$^+$ postmitotic neurons in the OB. This finding contradicted the normal finding that prenatal adverse stimulus impaired neurogenesis in postnatal brains [32-35].. To explore the basic molecular program that PNS employed to maintain stem cell proliferation in adult brains, we carried out bulk and single-nucleus RNAseq using E-SVZ tissues collected from control and stressed mouse brains. Gene regulatory network analysis indicated that PNS dysregulated the expression of genes that regulate cell cycle progression and neural stem cell maintenance, synapse organization and membrane potential, and gliogenesis. Particularly, we showed that the mild maternal stress at the mid-late stage of gestation sustained postnatal phosphorylation levels of MAPK3/1 in the E-SVZ, which in turn promoted NSC/NPC proliferation in adult male brains. This finding suggests that MAPK (ERK) is a bona fade downstream signaling cascade mediating extrinsic cues to stimulate cell proliferation in the adult brain. Furthermore, we found that prenatally stressed male mice had an intact olfactory function to locate food pellets and distinguish nonsocial odors, whereas they showed impairment in discriminating different social smells.

Results

PNS triggers cell proliferation in the lateral E-SVZ. To evaluate the effects of the prenatal aversive stimulus on cell proliferation in the E-SVZ, we employed a widely used stress-inducing method, the restraint stress on pregnant dams during the third week of gestation (60min/day, 0800h-0900h) [36]. The third week of gestation in mice roughly corresponds to the second trimester of human gestation, which is a critical period for the development of psychiatric disorders [37, 38]. To eliminate the postnatal influence from stressed mothers, the prenatally stressed (STR) pups were fostered by unstressed dams at postnatal day 0 (P0). As a control (CTL), pups from unstressed dams also underwent the fostering process. BrdU was administered by intraperitoneal (IP) injection one hour before tissue collection (Fig.1A).

Compared to the CTL, in STR male offspring the ratio of proliferating cells to the total number of cells in the lateral E-SVZ (MKI67$^+$ cells/total E-SVZ cells) was dramatically increased at P60 and P180, whereas similar increases were not detected in neonatal or juvenile mice (P0.5-21) (Fig.1B; Sup.Fig.1). We found that the numbers of BrdU$^+$/PROM1$^+$/GFAP$^-$ and MKI67$^+$/PROM1$^+$/GFAP$^-$ ependymal cells, and MKI67$^+$/DCX$^+$, BrdU$^+$/DCX$^+$, and MKI67$^+$/TUBB3$^+$ neuroblasts increased dramatically in STR male mice (Figs.1C, D, 2A; Sup.Fig.3A). This finding is in line with a previous study that showed ‘mild’ prenatal stress (30min/day, E15-17) enhanced neurogenesis in the DG of neonatal rat brains [39]. There were more BrdU$^+$ and MKI67$^+$ migrating neuroblasts in the rostral migratory stream (RMS) of stressed male mice than that of the CTL mice (Fig.2B). We did not observe statistically significant changes in the numbers of GFAP$^+$/BrdU$^+$ cells in either female or male offspring (Sup.Figs.2D, 3B).

In the female littermates, the changes were statistically insignificant, suggesting that female offspring were resilient to PNS (Sup.Figs.2, 3C,D). We found that under normal physiological conditions, the baseline of the

ratio of proliferating cells to total cells in the E-SVZ in female mice was higher than that of their male littermates ($BrdU^+/PROM1^+$ cells: female = 2.1 ± 0.4% vs. male = 0.9 ± 0.2%; $MKI67^+/PROM1^+$ cells: female = 4.1 ± 0.4% vs. male = 2.7 ± 0.3%. mean ± SEM). A similar finding was demonstrated in the subgranular zone of the hippocampal dentate gyrus in female mice by Tanapat et al [40]. Moreover, studies have shown that the influence of PNS exposure on the offspring is highly sex dependent. In rats, PNS significantly increased anxiety- and depression-related behaviors in male offspring, but not in female offspring [41, 42]. In humans, it has been shown that prenatal disturbances preferentially affect male offspring in a late-onset manner [43, 44].

E-SVZ NSC/NPC progenies migrate to and mature in the olfactory bulb (OB). To observe bulbar neurogenesis in the STR offspring, we labeled proliferating cells with two BrdU administrations separated by a 12-hr interval. The animals were sacrificed six weeks later (Fig.3A). BrdU-labeled cells migrated to the OB and mainly resided in the granule cell layer (GrO) with a few cells in the glomerular layer (Gl) and the external plexiform layer (EPl) in both CTL and STR offspring (8-9-month-old). As expected, the number of BrdU-labeled, newborn $RBFOX3^+$ neurons increased in the OB of stressed mice (Fig.3B, C). We did not observe substantial cell death in the OB of either the CTL or STR mice (Fig.3D).

Bulk and single nucleus RNAseq (snRNAseq) analyses show that PNS promotes E-SVZ cell proliferation via upregulating MAPK (ERK) pathway. In this study, we showed mild prenatal restraint stress enhanced the proliferation potency of NSC/NPCs in adult STR offspring. This finding contradicted the normal finding in the field that prenatal adverse stimulus impaired neurogenesis in postnatal brains [32, 33], suggesting that different stress levels ranging from mild to severe can have different negative influences on the neural development of offspring. To reveal the long-lasting molecular regulation that PNS elicited an increase in cell proliferation, we carried out transcriptomic analyses. Bilateral E-SVZ regions from 49 eight-month-old STR male and female mice were collected, rapidly frozen using liquid nitrogen, and stored at -80°C. Tissues from the left and right sides were stored separately: one for bulk RNAseq, and one for snRNAseq (Fig.4A).

Weighted gene co-expression network analysis and gene ontology (GO) enrichment analysis of bulk RNAseq data implied that PNS dysregulated gene expression networks related to the regulation of three biological functions: transferase activity (*Dusps1, 6, 5, Rgs, Spry2*; the purple module), cellular response to morphogens (*Shisa2*, *Ccn1*, *Spry2*, *Bambi*, *Smad7*; the purple module), and gliogenesis (*Mag*, *Trf*, *Myrf*, *Plp1*, *Gjc2*; the magenta module) in adult male offspring (Fig.4B, C). Many genes in the purple module are critical components of the RAS-RAF-MEK-MAPK(ERK) signaling cascade, which is the major downstream of growth factor signaling (e.g., EGF, FGF, VEGF) to promote cell proliferation [14, 18, 45-48]. GO enrichment analysis of the greenyellow and pink modules did not identify any signaling pathways. The major sex differences between males and females were the regulation of the immune effector process and cytokine production (the yellow module) (Fig.4B, C, Sup.Fig.5A) [49].

To further examine PNS-elicited changes in the E-SVZ, we carried out snRNAseq. The nuclei isolated from the E-SVZ cells of different litters were pooled, purified, and subjected to droplet-based snRNAseq (Fig.4A). Quality control filtering and integration of CTL and STR datasets were performed using the Seurat package[50] and the SingCellaR package [51, 52], which generated a merged dataset consisting of 7,407 cells and 20,634 genes for further analysis. According to marker gene expression, we annotated the 18 clusters to 10 different types of cells: 1) *Foxj1*$^+$ ependymal cell (EpC, cluster 6); 2) *Prom1*$^+$ endothelial-like cell (ElC, cluster 17); 3) dorsal neural progenitor cell (NPCd, cluster 14); 4) neuroblast (NB, clusters 7 and 11); 5) *Drd1*$^+$ spiny projection neuron (D1 SPN, clusters 2, 3, 10, 12); 6) *Drd2*$^+$ SPN (D2 SPN, clusters 1, 8, 13); 7) ventral neural progenitor cell (NPCv, cluster 16); 8) astrocyte (AC, clusters 4, 5); 9) oligodendrocyte (ODC, cluster 9) and oligodendrocyte precursor cell (OPC, cluster 18); 10) microglial cell (MG, cluster 15) (Fig.4D, Sup.Fig.5C). Cluster 11 NBs are dividing cells expressing *Mki67* and *Top2a*, while cluster 7 NBs are postmitotic cells. Cluster 14 NPCs express *Egfr*, *Mki67*, and *Btg2*, but not the NB markers *Dcx* and *Tubb3*. Astrocytes are separated into *Aqp4*$^-$ (cluster 4) and *Aqp4*$^+$ (cluster 5) cells. We detected a significant number of D1 and D2 SPNs that reside close to the E-SVZ (Sup.Fig.5B,C). Compared to the CTL, there were no obvious cell type changes in STR samples (Sup. Fig.4C).

To determine potential intrinsic programs that control NSC/NPC proliferation, we reanalyzed proliferating neural lineage cells. These cells express at least one of the cell cycle markers, *Mki67*, *Mcm2*, *Top2a*, and *Pcna* (UMI>0). We identified eight types of cells: EpC (cluster 7), ElC (cluster 8), NPC (cluster 3), NB (clusters 4 and 6), AC (cluster 5), D1 SPN (cluster 1), D2 SPN (cluster 2), and “eccentric” eSPN (cluster 9) (Fig.4E, Sup.Fig.5C) [53, 54]. Cell cycle position estimation analysis (estimating a continuous cell-cycle pseudotime by principal component analysis of cell-cycle genes) showed that most cells in cluster 3 (NPC), cluster 4 (NB), and some cells in cluster 8 (ElC) were actively dividing cells, while cells of other clusters were predicted to be in the G1-phase (Sup.Fig.5D, cell cycle score) [55]. Cells in cluster 3 (NPC, *Egfr*$^+$, *GFAP*$^-$*)* were likely to be the previously described activated NSC (aNSC) and/or transit-amplifying cells (TACs, C cells)[56]. Cluster 5 astrocytes expressed *Gfap* and *Pdgfrb*, but not *Egfr* and *Prom1*, suggesting an astroglial lineage (Sup.Fig.5B). It remains to be determined why a small subset of spiny projection neurons (D1, D2, and eSPN) expresses low levels of cell cycle markers. It seems that in addition to olfactory bulb neurons, this region could produce new striatal neurons [57]. Another possibility is that cells in or close to the E-SVZ could sense some environmental cues, and thus express cell cycle markers.

We next employed the bigSCale2 algorithm to construct gene regulatory networks for the proliferating cells[58] (Fig. 4F). Compared to the CTL network, the STR network showed a lower edge-to-node density (gene to gene interaction across functional networks (module)) (CTL = 8.17, STR = 7.63) and higher modularity (gene to gene interaction within a module) (CTL = 0.41, STR = 0.54), suggesting that PNS caused a sparser network with a higher gene expression heterogeneity in the E-SVZ of STR offspring. The analysis

implicated two major network modules that regulate cell cycle progression and neural circuit maturation (Fig.4F). GO analysis of differentially expressed hub genes showed that PNS promoted the expression of genes that regulated cell cycle progression (e.g., *Atad2*, *Top2a*, *Brd8*, *Atad5*, *Smchd1*, *Ncapg2*, *Pola1*, *Ezh2*) and neural stem cell maintenance and differentiation (e.g., *Sox2*, *Sox5*, *Nfib*, Zmiz1, *Zeb2*), while it downregulated expression levels of genes modulating synapse organization and membrane potential (e.g., *Slc8a2*, *Kcnd2*, *Grm5*, *Nfia*, *Ntrk3*, *Slit3*) (Fig.4F,G). More specifically, PNS enhanced the expression of bromodomain-containing genes *Atad2* (ATPase family AAA domain containing 2) and *Brd8* (bromodomain containing 8) that are involved in ESR1 (estrogen receptor alpha) mediated transcriptional regulation of cell proliferation in cancer cell lines [59-61]. PNS increased expression levels of Wnt pathway modulators *Ezh2*, *Tcf4*, *Ephb2*, and *Sox2*, which play important roles in sustaining cell stemness and promoting cell proliferations [62-66]. The Wnt and the estrogen signaling pathways are tightly associated with MAPK3/1 (ERK1/2) signaling to stimulate tumorigenesis [26, 67, 68]. Moreover, MAP4K4 (serine/threonine kinase mitogen-activated protein 4 kinase 4) has been identified as a positive regulator of MAPK (ERK) signaling in cancer cells[68]. In addition, previous studies by our group and others have shown that MAPK3/1 are essential in maintaining the proliferation of adult NSC/NPCs [69-71]. Considering the above transcriptomic analysis, we hypothesized that PNS promoted cell proliferation via the activation of the MAPK (ERK) signaling in the E-SVZ NSC/NPCs of adult male offspring (Sup.Fig.6A).

Rescue assays reveal that PNS upregulates MAPK3/1 phosphorylation To test this hypothesis, we first carried out an immunostaining assay to examine phosphorylation levels of MAPK3/1 in the E-SVZ of both CTL and STR mice. The antibody was developed to recognize phosphorylated MAPK3/1 at threonine 202/185 and tyrosine 204/187 loci specifically (ThermoFisher 44-680G). We found that immunostaining of phosphorylated MAPK (p-MAPK) showed a punctate pattern (Figs.5A, 6B). This pattern was affirmed by using another p-MAPK3/1 specific antibody from a different vendor (Cell Signaling, 4370) and an antibody against unphosphorylated MAPK(ERK) (Cell Signaling, 4695) (Sup.Fig.6B, C). Furthermore, when treating the section with lambda protein phosphatase (Lambda PP) before primary antibody incubation, the immunoreactivity of the p-MAPK3/1 antibody was completely abolished, suggesting the high specificity of the antibody in recognizing p-MAPK (Sup.Fig.6D).

Since both phosphorylated and unphosphorylated MAKP3/1 staining displayed punctate patterns, we reasoned that the number of puncta correlates with the status of phosphorylation. By employing this quantitative methodology, we next examined the phosphorylation of MAPK3/1 in the E-SVZ at different postnatal developmental time points (P0.5-180). Concomitant with the cell proliferation finding (Fig.1B), we found phosphorylation level of MAPK3/1 was considerably upregulated in the E-SVZ of stressed adult offspring (P60, P180) but not at earlier stages (Fig.5).

To definitively verify the role of the MAPK3/1 pathway in regulating cell proliferation in stressed male mice, we carried out rescue assays by treating the STR and CTL animals with a selective phosphorylated MAPK3/1 inhibitor, LY3214996, and an inhibitor of upstream protein kinases MAP2K1/2 (MEK1/2), GSK1120212. We found that administration of these inhibitors effectively reduced the numbers of p-MAPK3/1 puncta and proliferating cells in the E-SVZ of both CTL and STR mice (Fig.6). Taken together, the rescue assays suggested that MAPK(ERK) signaling played a critical role in promoting NSC/NPC proliferation in STR adult male mice.

Discussion

Psychosocial, cultural, and environmental stressors experienced during gestation can be detrimental to pregnancy as well as maternal and fetal health. Recent studies have suggested that prenatal maternal stress can shape neural circuitry, neural cell fate, and behavior in offspring, which may set the stage for postnatal disease vulnerability [7, 9-11]. Neural stem cells in the adult central nervous system are highly sensitive to environmental stimuli. For example, neural stem cells can rapidly respond to brain and spinal cord injuries and mitogen stimulation (e.g., EGF, VEGF, and FGF) to proliferate [14, 18, 72, 73]. Moreover, under normal physiological conditions in rodents, growth factors EGF and VEGF have been shown to activate dormant/quiescent proliferation [14, 72]. In the current study, we showed the long-lasting response of neural stem cells in STR offspring to a prenatal adverse stimulus, restraint stress. Our data suggested that in adult STR offspring, cells in the stem cell niche E-SVZ responded to the stress through enhancing growth factors-, Wnt-, and estrogen-regulated pathways, and the MAPK (ERK) signaling cascade could be the central player that mediates the long-lasting effect of the prenatal event.

It has now been accepted that adult neurogenesis happens in mammals despite some disputes over the origin of neural stem cells in rodent brains and the existence of neurogenesis in humans [14, 15, 18, 48, 71, 74-77]. In mammals, the current theory of adult neurogenesis is adopted from the well-established embryonic neurogenesis paradigm that neurons and glial cells are generated from sequential symmetrical or asymmetrical divisions of neuroepithelial cells/radial glia and then intermediate progenitors [78-80]. Our snRNAseq analysis suggested that PNS upregulated the expression level of *Zeb2* (zinc finger E-box binding homeobox 2) and its downstream target *Sox6* in the germinal zone of adult STR brains [81] (Fig.4F). ZEB2 is one of the essential transcription factors that induce epithelial-mesenchymal transition (EMT) during pluripotent stem cell differentiation, embryonic development, wound healing, and tumorigenesis [82-84]. Studies by Miquelajauregui et al. and Deryckere et al. found that ZEB2 plays a critical role in controlling neurogenesis in prenatal and postnatal brains, respectively [81, 85]. Moreover, Wnt and MAPK (ERK) pathways have been shown to induce *Zeb2* expression and promote EMT in cancer cells [82, 83]. MAPK(ERK) is a potent signaling transducer of EGF and VEGF, which are essential for promoting dormant or quiescent neural stem cell activation and neural

progenitor cell proliferation [14, 19, 24, 46, 70-72]. Therefore, PNS could activate dormant/quiescent neural stem cell proliferation via promoting MAPK (ERK)-mediated EMT in the germinal zones of the adult brain.

To examine the possible association between PNS and basic olfactory function, we carried out the buried food test and the habituation/dishabituation test. Our initial study showed that STR male mice (5-8-month-old) had a largely intact olfactory function to locate food pellets and discriminate nonsocial odors, while the STR mice showed impairment in the differentiation of different social odors and habituation of social odor 2 (STR Social 1-3 median=2.98 sec to Social 2-1 median=2.58 sec; CTL Social 1-3 median=1.34 sec to Social 2-1 median=4.66 sec) (Sup.Fig.4B-D). Calbindin 2 (CALB2, a.k.a. Calretinin) staining showed a disorganized glomerular layer (Gl) and a slightly increased number of $CALB2^{+}$ cells in the external plexiform layer (EPl) and the granule cell layer (GrO) of the OB in stressed male mice (Sup.Fig.4A). Glomeruli and granular cells have been shown to play essential roles in the regulation of olfactory habituation behavior [86, 87]. Moreover, scRNAseq analysis showed that PNS attenuated the expression of genes modulating synapse organization and membrane potential, which may affect olfactory functions (Fig.4G). For example, PNS downregulated the expression of glutamate metabotropic Receptor 5 (*Grm5*, a.k.a. mGluR5), which has been shown to regulate granule cell-mediated inhibition and odor discrimination [88, 89]. Taken together, although the causal relationship between increased NSC/NPC proliferation and the behavioral deficit is still elusive, BrdU lineage tracing together with immunostaining showed disorganized cytoarchitecture of the olfactory glomerular layer and slightly increased numbers of CALB2+ cells in the external plexiform layer and the granule cell layer, which have been shown to play essential roles in the regulation of olfactory habituation behavior [90-93].

Materials and Methods

Experimental Animals. Mice were kept and fed in standard conditions on a 12hr light/dark cycle. Experimental procedures on animals were performed following the guidelines of the University of California, Los Angeles (UCLA) Institutional Animal Care and Use Committee and UCLA Animal Research Committee, and the Regional Committee for Medical Research Ethics of Tongji University. The inbred strain C57BL⁄6NCrlVr mice were used in this study. Pregnancy was timed by daily monitoring for vaginal plugs.

Restraint stress and tissue collection. To induce stress between gestational days 14 and delivery (~E19.5), the pregnant dam was placed individually in a plastic restrainer fitted closely to body size for 60 min/day (session at 0800h). Control pregnant females were left undisturbed in their home cages. After delivery, the prenatally stressed (STR) and the CTL pups were fostered by unstressed, same strain mothers at P0. All pups were weaned at P21. For tissue collection, the animals were sacrificed, and their brains were removed for immunostaining or RNA sequencing.

Buried food and olfactory habituation/dishabituation tests. The tests were described by Yang and Crawley[94]. Details are given in SI Appendix.

Bromodeoxyuridine (BrdU) administration. The BrdU injection was described in our previous study[50]. Details are given in SI Appendix.

Immunohistochemistry. The primary antibodies used in this study were BrdU (Abcam ab6326, 1:100; ab1893 1:250), MKI67 (Abcam ab15580, 1:200), GFAP (ThermoFisher PA1-10004, 1:500), TUBB3 (R&D MAB1195, 1:500), CALB2 (Synaptic Systems 214111, 1:200), DCX (Santa Cruz sc-8066, 1:400), RBFOX3 (Abcam ab177487, 1:500), p-MAPK3/1(ThermoFisher 44-680G, 1:100), p-MAPK3/1 (Cell Signaling 4370, 1:200), and MAPK3/1 (Cell Signaling 4695, 1:250). Fluorophore-conjugated secondary antibodies were purchased from ThermoFisher Scientific and Jackson ImmunoResearch.

Terminal deoxynucleotidyl transferase dUTP Nick-End Labeling (TUNEL) assay. TUNEL assay was carried out following the manufacturer's instructions (*In Situ* Cell Death Detection Kit, Roche-11684795910).

Tissue processing for BrdU immunostaining. Details are given in SI Appendix.

Transcriptomic analysis. The brains of 7- or 8-month-old STR and CTL offspring were sectioned at 300μm thickness in artificial cerebrospinal fluid supplied with actinomysin D (3μM, Sigma-Aldrich). The lateral walls of ependymal SVZ (E-SVZ) were dissected, frozen in liquid nitrogen, and stored in air-tight tubes in -80°C freezer.

Bulk RNAseq. Total RNA was extracted and purified using RNeasy Mini Kit (Qiagen 74104). 100ng of qualified RNA was subjected to VAHTS™ mRNA-seq V3 Library Prep Kit for Illumina® (Vazyme NR611) for library preparation, followed by quality assessment using Agilent Bioanalyzer 2100, and sequencing on Illumina NovaSeq 6,000. The mRNA sequencing reads were mapped to the mouse reference genome (GRCm38) using HISAT2 (version 2.2.1) and StringTie (version 2.1.4), and the mapped reads were assigned using featureCounts function of R package Rsubread (version 2.0.1). The counts were normalized using the DESeq2 R package (version 1.30.0)[95]. Pseudogenes (gene names with the prefix "Gm") were filtered out, and top 10,000 highly variable genes were kept for weighted gene co-expression network analysis (WGCNA) using the R package WGCNA (version 1.69)[96]. Specifically, a soft-power of 12 was chosen to construct a topological overlap matrix from the gene correlation network. Modules were determined by the Dynamic Hybrid Cut algorithm using a "deepSplit" parameter of 2. Highly correlated modules (Pearson correlation of module

eigengene > 0.9) were merged as one module using a “mergeCutHeight” parameter of 0.25. Gene ontology (GO) and KEGG pathway enrichment analyses of genes in each identified module were performed using the R package clusterProfiler (version 4.4.4)[97] set at default parameters.

Single nucleus RNAseq (snRNAseq). Single nuclei were extracted from pooled frozen lateral walls of ependymal SVZ (E-SVZ) from CTL and STR mice using a previously described ultracentrifugation method[98] with some modifications. The single nuclei RNA sequencing library construction was performed using the Chromium Next GEM Single Cell 3’ Reagent Kits v3.1 (10× Genomics) according to the user guide. The quality assessment of the libraries was conducted using Agilent Bioanalyzer 2100, and the sequencing was performed on an Illumina Novaseq 6000. The alignment, filtering, barcode assignment, and UMI counting of the sequenced reads were processed using the Cell Ranger pipeline (version 5.0.1, 10× Genomics). Quality control (QC) of cells and genes was performed using R package Seurat (version 4.1.1). Doublets were removed using R package scDblFinder (version 1.10.0). Additional downstream workflow (including further QC, sample integration, highly variable gene selection, dimensional reduction, clustering, cluster marker gene identification, and visualization) was processed via SingCellaR R package (version 1.2.1)[51, 52]. According to the expression of the marker genes, along with well-established celltype specific gene sets, the 18 clusters were assigned to 11 major celltypes: dorsal neural progenitor cells (NPCd), ventral neural progenitor cells (NPCv), neuroblasts (NB), astrocytes (AC), ependymal cells (EpC), endothelia-like cells (ElC), *Drd1*$^{+}$ SPN (D1), *Drd2*$^{+}$ SPN (D2), oligodendrocyte progenitor cells (OPC), oligodendrocytes (ODC), and microglia (MG).

Cells (except for clusters without neuronal lineage potential, OPC, ODC and MG) expressing at least one of the four cell cycle-related genes (*Mki67*, *Top2a*, *Mcm2*, and *Pcna*) were isolated and re-clustered via SingCellaR workflow. The potentially dividing cells were clustered into 9 clusters and annotated as neural progenitor cells (NPC), AC, NB, EpC, ElC, D1, D2, “eccentric” spiny projection neuron (eSPN), respectively. The cell-cycle position of each potentially dividing cell was estimated using the tricycle R package (version 1.4.0)[55]. The putative gene-to-gene correlated network of the potential dividing cells was inferred using the bigSCale2 algorithm (version 2.0)[58]. The network centrality PageRank (PR) was chosen to represent gene essentiality. Gene communities in each network were identified, and those communities consisting of over 5 genes were considered as main communities. Hub genes with maximal biological relevance in each main community were defined as the intersection of three gene sets: 1) top 500 genes with the biggest change in PR absolute value between STR and CTL; 2) genes with over 0.75 quantile of PR value; 3) DEGs between STR and CTL determined using SingCellaR package (version 1.2.1)[51, 52]. GO enrichment analysis of the hub genes was performed using R package clusterProfiler (version 4.4.4)[97] set at default parameters. Details are given in SI Appendix.

Rescue assay. A MAPK3/1 inhibitor LY3214996 (Selleck, 16 mg/kg) and a MAP2K1/2 inhibitor GSK1120212 (Selleck, 0.35 mg/kg), and the vehicle solution were daily intraperitoneally (IP) injected to 9- to 10-month-old prenatally stressed male offspring for 27 days (except for the 11th and 22nd days), respectively. Details are given in SI Appendix.

Lambda Protein Phosphatase (Lambda PP) reaction. The assay was carried out following the manufacturer's instructions (NEB, P0753S). Details are given in SI Appendix.

Imaging and Statistical Analysis. At least three mice of each gender from different litters at different postnatal stages were randomly selected for immunostaining and quantification analysis. Stained sections were imaged with Zeiss LSM800 confocal microscope as tiled or single images. Images obtained were processed and quantified with Imaris software and ImageJ. Statistical analyses of the data were carried out with R-package, GraphPad Prism, and SAS (Statistical Analysis Software). Mann-Whitney test was used to assess statistical significance between independent experimental groups. All reported significant levels to represent two-tailed values. Details are given in SI Appendix.

Figure legends

Fig. 1. PNS promoted PROM1^{+} cell proliferation in the lateral E-SVZ of prenatally stressed male offspring. (A) The pregnant dams were stressed in a plastic restrainer from E14 until delivery. Samples were collected at postnatal different time points. To label proliferating cells, BrdU was IP injected 1hr before sacrifice. **(B)** PNS significantly increased E-SVZ NSC proliferation in prenatally stressed adult offspring (P60 and P180), but not neonatal and juvenile mice (P0.5-21). CPu, caudate putamen; LV, lateral ventricle; Sept, septum. Scale bar, 30 μm. **(C)** MKI67 (green color), PROM1 (red color), and GFAP (white color) immunostaining. The enlarged images at the bottom showed MKI67^{+}/PROMl^{+} ependymal cells are GFAP negative (MKI67^{+} cells: CTL = 24.5 ± 1.6%, n = 6; STR = 31.8 ± 2.8%, n=6. P = 0.026. MKI67^{+}/PROM1^{+} cells: CTL = 2.7 ± 0.3%, n = 13; STR= 5.5 ± 0.8%, n = 10. P = 0.0002). The box plot showed the minimum, the maximum, the median, the mean (the + symbol), and the first and the third quartiles. Scale bars, 10 μm, 2 μm. **(D)** BrdU (green color), PROM1 (red color), and GFAP (white color) immunostaining (BrdU^{+} cells: CTL = 13.3 ± 0.9%, n = 28; STR =21.4 ± 1.4%, n = 26. P<0.0001. BrdU^{+}/PROM1^{+} cells: CTL = 0.9 ± 0.2%, n = 26; STR = 2.9 ± 0.5%, n = 18. P = 0.0002). The enlarged images on the bottom showed BrdU/PROMl double positive ependymal cells were GFAP negative. Scale bars, 10 μm, 2 μm. CTL, control; STR, stressed. Mann-Whitney test. All data were presented as mean ± SEM. *p < 0.05, ***p < 0.001, ****p < 0.0001. For sample

quantification, we examined sections collected from minimal 3-5 brains of different litters per experimental condition.

Fig. 2. PNS promotes neuroblast proliferation in the E-SVZ and the RMS of male offspring. (A) MKI67/BrdU/DCX immunostaining shows that the ratio of neuroblasts increased dramatically in the lateral E-SVZ ($BrdU^+/DCX^+$ cells: CTL = 3.5 ± 0.4%, n = 21; STR = 7.0 ± 0.6%, n = 23. P<0.0001. $MKI67^+/DCX^+$ cells: CTL = 11.8 ± 1.3%, n = 21; STR = 17.3 ± 1.3%, n = 23. P = 0.0071). Scale bars, 30 μm. **(B)** The ratio of proliferating A-cell ($BrdU^+$ or $MKI67^+$) increased in the RMS ($MKI67^+$ cells: CTL = 27.3 ± 1.8%, n = 38; STR = 35.1 ± 1.4%, n = 40. P = 0.0021. $BrdU^+$ cells: CTL = 14.6 ± 1.1%, n = 38; STR = 17.3 ± 0.6%, n = 40. P = 0.021). Scale bars, 100 μm. Mann-Whitney test. All data were presented as mean ± SEM. *p < 0.05, **p < 0.01, ****p < 0.0001.

Fig. 3. PNS disturbs bulbar neurogenesis. **(A)** To determine fates of lateral E-SVZ NSCs in prenatally stressed male mice, NSCs were labeled with two BrdU IP injections. After 6 weeks, the brain samples were collected. **(B)** BrdU immunostaining (white color). The enlarged images on the right show BrdU staining in the GrO ($BrdU^+$ cells/OB section: CTL = 92 ± 8, n = 8. STR = 166 ± 19, n =8. P = 0.0011. **p < 0.01. mean ± SEM). Mann-Whitney test. Scale bar, 200 μm. **(C)** BrdU labeled cells migrated to the OB and matured to become $RBFOX3^+$ neurons. The arrowheads show BrdU/RBFOX3 double-positive cells in the GrO. Scale bars, 200 μm. **(D)** TUNEL assay shows that PNS does not cause cell apoptosis in the OB. Scale bars, 300 μm. GrO, granular cell layer of OB; Mi, mitral cell layer; EPl, external plexiform layer; Gl, glomerular layer.

Fig. 4. Bulk and single nucleus transcriptomic analyses of cells in the lateral E-SVZ of STR and CTL mice. (A) Schematic overview of tissue and single nucleus isolation for bulk RNA sequencing and single nucleus RNA sequencing (snRNAseq). **(B)** Module-trait correlation analysis revealed 3 modules in male offspring were correlated with PNS (Magenta, Greenyellow, Purple). **(C)** GO analysis shows top 7 GO terms enriched in major gene modules (Magenta and Purple), excluding redundant terms. The top 5 enriched genes of each term are listed. **(D)** Force-directed graph is used to visualize clusters of the total single nucleus dataset (the left panel). EpC, ependymal cell; ElC, endothelial-like cell; NPCd, dorsal neural progenitor cell; NPCv, ventral neural progenitor cell; NB, neuroblast; D1, dopamine receptor D1, $Drd1^+$ spiny projection neuron; D2, $Drd2^+$ spiny projection neuron; AC, astrocyte; OPC, oligodendrocyte progenitor cell; OD, oligodendrocyte; MG, microglia. The violin plot (the right panel) shows the top cell-type-specific genes expressed in the clusters defined in the left panel. **(E)** Force-directed graph drawing of the potentially dividing cells dataset (the left panel), and the violin plot (the right panel) of the expression of cell-type marker genes. MCM2, minichromosome maintenance complex component 2; TOP2A, DNA topoisomerase II alpha; PCNA,

proliferating cell nuclear antigen; eSPN, “eccentric” spiny projection neuron. The expression of top cell-type-specific genes of each cluster is shown in the right panel. **(F)** Gene regulatory network analysis of proliferating cells (E). The node size is proportional to its PageRank (PR) centrality. Nodes highlighted in darkorange/cadetblue colors in the network indicate genes in the intersection of three gene sets: 1) top 500 genes with the biggest changes in PR absolute value between STR and CTL; 2) genes with over 0.75 quantile of PR value in each main community (community consisting of over 5 genes) detected in the network; 3) DEGs between STR and CTL. The Nodes with text labels refer to hub genes with maximal biological relevance. **(G)** Bar plots show the GO enrichment results of up- and down-regulated hub genes in (F).

Fig. 5. MAPK3/1 phosphorylation in developing and adult brains. MAPK3/1 phosphorylation showed a dramatic difference between CTL and STR at P180 and P60, but not in samples collected from P0.5 to P21. At each time point, the panels on the right showed an enlarged area labeled in the left panels. Scale bars, 10 μm, 1 μm (zoomed-in images). Mann-Whitney test. All data were presented as mean ± SEM. *p < 0.05, **p < 0.01.

Fig. 6. Inhibition of MAPK activity counteracts PNS-triggered NSC/NPC proliferation in the lateral E-SVZ. (A, B) Administration of MAPK3/1 inhibitor LY3214996 (LY) and MAP2K1/2 inhibitor GSK1120212 (GSK) decreases the total phosphorylated MAPK3/1 puncta in the E-SVZ (CTL = 6.2 ± 0.3, n = 18; CTL/LY = 5.1 ± 0.5, n = 16; CTL/GSK = 5.3 ± 0.2, n = 17; STR = 8.7 ± 0.5, n = 16; STR/LY = 4.2 ± 0.3, n = 16; STR/GSK = 7.2 ± 0.3, n = 15. CTL vs LY, P = 0.0056; CTL vs GSK, P = 0.0032; CTL vs STR, P = 0.0002; STR vs LY, P < 0.0001; STR vs GSK, P = 0.0405). Scale bars, 30 μm. **(C)** Inhibition of MAPK pathway reduces the number of both $PROM1^+/MKI67^+$ ependymal cells and $TUBB3^+/MKI67^+$ neuroblasts. $MKI67^+$cells: CTL = 20.7 ± 0.8%, n = 18; CTL/LY = 17.3 ± 1.0%, n = 15; CTL/GSK = 14.1 ± 1.6%, n = 12; STR = 29.2 ± 1.7%, n = 24; STR/LY = 20.3 ± 0.8%, n = 38; STR/GSK = 22.4 ± 0.9%, n = 38. CTL vs LY, P = 0.0229; CTL vs GSK, P = 0.0008; STR vs LY, P < 0.0001; STR vs GSK, P = 0.0013. $PROM1^+/MKI67^+$ cells: CTL = 1.8 ± 0.3%, n = 16; CTL/LY = 1.4 ± 0.2%, n = 15; CTL/GSK = 1.4 ± 0.5%, n = 12; STR = 2.9 ± 0.4%, n = 20; STR/LY = 0.8 ± 0.2%, n = 17; STR/GSK = 1.0 ± 0.2%, n = 14. CTL vs LY, P = 0.5263; CTL vs GSK, P = 0.3770; STR vs LY, P < 0.0001; STR vs GSK, P < 0.0001. $TUBB3^+/MKI67^+$ cells: CTL = 10.6 ± 0.6%, n = 18; CTL/LY = 7.9 ± 0.7%, n = 15; CTL/GSK = 6.0 ± 0.5%, n = 12; STR = 14.3 ± 0.8%, n = 20; STR/LY = 11.7 ± 0.7%, n = 17; STR/GSK = 9.1 ± 1.0%, n = 14. CTL vs LY, P = 0.0091; CTL vs GSK, P < 0.0001; STR vs LY, P < 0.0151; STR vs GSK, P < 0.0010. Scale bars, 30 μm. Mann-Whitney test. All data were presented as mean ± SEM. *p < 0.05, **p < 0.01, ***p < 0.001, ****p < 0.0001.

Acknowledgments

The study was supported by the National Key Research and Development Program of China (2020YFC2002804), NIH Grants (5R21MH115382, U54HD087101, and P50HD103557), State Key Program of the National Natural Science Foundation of China (82030035), the Foundation of Shanghai Municipal Education Commission (2019-01-07-00-07-E00055), Peak Disciplines (Type IV) of Institutions of Higher Learning in Shanghai, Postdoctoral Science Foundation funded project (2022M712418), the 2021 Shanghai "Super Postdoctoral" Incentive Program, Key R&D Program of Jiangsu (BE2020026), and National Natural Science Foundation of China (31872761). We thank the Intellectual and Developmental Disabilities Research Center at the University of California, Los Angeles.

Conflict of Interest

All authors declare that they have no conflicts of interest.

References

1. Marco EM, Macri S, Laviola G. Critical age windows for neurodevelopmental psychiatric disorders: evidence from animal models. Neurotox Res. 2011;19(2):286-307. Epub 2010/07/08. doi: 10.1007/s12640-010-9205-z. PubMed PMID: 20607469.

2. Dehorter N, Vinay L, Hammond C, Ben-Ari Y. Timing of developmental sequences in different brain structures: physiological and pathological implications. Eur J Neurosci. 2012;35(12):1846-56. Epub 2012/06/20. doi: 10.1111/j.1460-9568.2012.08152.x. PubMed PMID: 22708595.

3. Weinstock M. Prenatal stressors in rodents- Effects on behavior. Neurobiology of Stress. 2017;6:3-13. doi: 0.1016/j.ynstr.2016.08.004.

4. Stevens HE, Su T, Yanagawa Y, Vaccarino FM. Prenatal stress delays inhibitory neuron progenitor migration in the developing neocortex. Psychoneuroendocrinology. 2013;38(4):509-21. doi: 10.1016/j.psyneuen.2012.07.011. PubMed PMID: 22910687; PubMed Central PMCID: PMCPMC3532962.

5. Rothenberger SE, Moehler E, Reck C, Resch F. Prenatal stress: course and interrelation of emotional and physiological stress measures. Psychopathology. 2011;44(1):60-7. Epub 2010/11/13. doi: 000319309 [pii] 10.1159/000319309. PubMed PMID: 21072001.

6. Uchida T, Furukawa T, Iwata S, Yanagawa Y, Fukuda A. Selective loss of parvalbumin-positive GABAergic interneurons in the cerebral cortex of maternally stressed Gad1-heterozygous mouse offspring. Transl Psychiatry. 2014;4:e371. doi: 10.1038/tp.2014.13. PubMed PMID: 24618690; PubMed Central PMCID: PMCPMC3966041.

7. Mychasiuk R, Gibb R, Kolb B. Prenatal stress alters dendritic morphology and synaptic connectivity in the prefrontal cortex and hippocampus of developing offspring. Synapse. 2012;66(4):308-14. Epub 2011/11/29. doi: 10.1002/syn.21512. PubMed PMID: 22121047.

8. Sadler TR, Nguyen PT, Yang J, Givrad TK, Mayer EA, Maarek JM, et al. Antenatal maternal stress alters functional brain responses in adult offspring during conditioned fear. Brain Res. 2011;1385:163-74. Epub 2011/02/09. doi: 10.1016/j.brainres.2011.01.104. PubMed PMID: 21300034; PubMed Central PMCID: PMC3065538.

9. Li Y, Sjölander A, Song H, Cnattingius S, Fang F, Yang Q, et al. Associations of parental and perinatal factors with subsequent risk of stress-related disorders: a nationwide cohort study with sibling comparison. Molecular Psychiatry. 2022. doi: 10.1038/s41380-021-01406-5.

10. Lupien SJ, McEwen BS, Gunnar MR, Heim C. Effects of stress throughout the lifespan on the brain, behaviour and cognition. Nat Rev Neurosci. 2009;10(6):434-45. Epub 2009/04/30. doi: nrn2639 [pii] 10.1038/nrn2639. PubMed PMID: 19401723.

11. Robinson R, Lahti-Pulkkinen M, Heinonen K, Reynolds RM, Räikkönen K. Fetal programming of neuropsychiatric disorders by maternal pregnancy depression: a systematic mini review. Pediatric Research. 2019;85(2):134-45. doi: 10.1038/s41390-018-0173-y.

12. Allen E. The cessation of mitosis in the central nervous system of the Albino rat. Journal of Comparative Neurology. 1912;22(6):547-68.

13. Altman J, Das GD. Autoradiographic and histological evidence of postnatal hippocampal neurogenesis in rats. Journal of Comparative Neurology. 1965;124(3):319-35. doi: https://doi.org/10.1002/cne.901240303.

14. Luo Y, Coskun V, Liang A, Yu J, Cheng L, Ge W, et al. Single-cell transcriptome analyses reveal signals to activate dormant neural stem cells. Cell. 2015;161(5):1175-86. Epub 2015/05/23. doi: 10.1016/j.cell.2015.04.001. PubMed PMID: 26000486; PubMed Central PMCID: PMCPMC4851109.

15. Doetsch F, Caille I, Lim DA, Garcia-Verdugo JM, Alvarez-Buylla A. Subventricular zone astrocytes are neural stem cells in the adult mammalian brain. Cell. 1999;97(6):703-16. Epub 1999/06/25. doi: 10.1016/s0092-8674(00)80783-7. PubMed PMID: 10380923.

16. Eriksson PS, Perfilieva E, Bjork-Eriksson T, Alborn AM, Nordborg C, Peterson DA, et al. Neurogenesis in the adult human hippocampus. Nat Med. 1998;4(11):1313-7. Epub 1998/11/11. doi: 10.1038/3305. PubMed PMID: 9809557.

17. Gould E, Tanapat P, McEwen BS, Flugge G, Fuchs E. Proliferation of granule cell precursors in the dentate gyrus of adult monkeys is diminished by stress. Proc Natl Acad Sci U S A. 1998;95(6):3168-71. Epub 1998/04/18. doi: 10.1073/pnas.95.6.3168. PubMed PMID: 9501234; PubMed Central PMCID: PMCPMC19713.

18. Johansson CB, Momma S, Clarke DL, Risling M, Lendahl U, Frisén J. Identification of a neural stem cell in the adult mammalian central nervous system. Cell. 1999;96(1):25-34. Epub 1999/02/16. doi: 10.1016/s0092-8674(00)80956-3. PubMed PMID: 9989494.

19. Delgado AC, Maldonado-Soto AR, Silva-Vargas V, Mizrak D, von Kanel T, Tan KR, et al. Release of stem cells from quiescence reveals gliogenic domains in the adult mouse brain. Science. 2021;372(6547):1205-9. Epub 2021/06/12. doi: 10.1126/science.abg8467. PubMed PMID: 34112692.

20. Lois C, Alvarez-Buylla A. Proliferating subventricular zone cells in the adult mammalian forebrain can differentiate into neurons and glia. Proceedings of the National Academy of Sciences of the United States of America. 1993;90(5):2074-7. doi: 10.1073/pnas.90.5.2074. PubMed PMID: 8446631.

21. Pilz GA, Bottes S, Betizeau M, Jörg DJ, Carta S, Simons BD, et al. Live imaging of neurogenesis in the adult mouse hippocampus. Science. 2018;359(6376):658-62. Epub 2018/02/14. doi: 10.1126/science.aao5056. PubMed PMID: 29439238; PubMed Central PMCID: PMCPMC6986926.

22. Altman J, Das GD. Autoradiographic and histological evidence of postnatal hippocampal neurogenesis in rats. J Comp Neurol. 1965;124(3):319-35. Epub 1965/06/01. doi: 10.1002/cne.901240303. PubMed PMID: 5861717.

23. Zhang W, Liu HT. MAPK signal pathways in the regulation of cell proliferation in mammalian cells. Cell Research. 2002;12(1):9-18. doi: 10.1038/sj.cr.7290105.

24. Lavoie H, Gagnon J, Therrien M. ERK signalling: a master regulator of cell behaviour, life and fate. Nat Rev Mol Cell Biol. 2020;21(10):607-32. Epub 2020/06/25. doi: 10.1038/s41580-020-0255-7. PubMed PMID: 32576977.

25. Rovida E, Stecca B. Mitogen-activated protein kinases and Hedgehog-GLI signaling in cancer: A crosstalk providing therapeutic opportunities? Semin Cancer Biol. 2015;35:154-67. Epub 2015/08/21. doi: 10.1016/j.semcancer.2015.08.003. PubMed PMID: 26292171.

26. Atanaskova N, Keshamouni VG, Krueger JS, Schwartz JA, Miller F, Reddy KB. MAP kinase/estrogen receptor cross-talk enhances estrogen-mediated signaling and tumor growth but does not confer tamoxifen

resistance. Oncogene. 2002;21(25):4000-8. Epub 2002/05/31. doi: 10.1038/sj.onc.1205506. PubMed PMID: 12037682.

27. Yun MS, Kim SE, Jeon SH, Lee JS, Choi KY. Both ERK and Wnt/beta-catenin pathways are involved in Wnt3a-induced proliferation. J Cell Sci. 2005;118(Pt 2):313-22. Epub 2004/12/24. doi: 10.1242/jcs.01601. PubMed PMID: 15615777.

28. Katz M, Amit I, Yarden Y. Regulation of MAPKs by growth factors and receptor tyrosine kinases. Biochim Biophys Acta. 2007;1773(8):1161-76. Epub 2007/02/20. doi: 10.1016/j.bbamcr.2007.01.002. PubMed PMID: 17306385; PubMed Central PMCID: PMCPMC2758354.

29. Hartsough MT, Frey RS, Zipfel PA, Buard A, Cook SJ, McCormick F, et al. Altered transforming growth factor signaling in epithelial cells when ras activation is blocked. J Biol Chem. 1996;271(37):22368-75. Epub 1996/09/13. doi: 10.1074/jbc.271.37.22368. PubMed PMID: 8798398.

30. Shin S, Dimitri CA, Yoon S-O, Dowdle W, Blenis J. ERK2 but Not ERK1 Induces Epithelial-to-Mesenchymal Transformation via DEF Motif-Dependent Signaling Events. Molecular Cell. 2010;38(1):114-27. doi: https://doi.org/10.1016/j.molcel.2010.02.020.

31. Gonzalez DM, Medici D. Signaling mechanisms of the epithelial-mesenchymal transition. Sci Signal. 2014;7(344):re8. Epub 2014/09/25. doi: 10.1126/scisignal.2005189. PubMed PMID: 25249658; PubMed Central PMCID: PMCPMC4372086.

32. Lemaire V, Koehl M, Le Moal M, Abrous DN. Prenatal stress produces learning deficits associated with an inhibition of neurogenesis in the hippocampus. Proc Natl Acad Sci U S A. 2000;97(20):11032-7. Epub 2000/09/27. doi: 97/20/11032 [pii]. PubMed PMID: 11005874; PubMed Central PMCID: PMC27143.

33. Belnoue L, Grosjean N, Ladeveze E, Abrous DN, Koehl M. Prenatal stress inhibits hippocampal neurogenesis but spares olfactory bulb neurogenesis. PloS one. 2013;8(8):e72972. Epub 2013/09/07. doi: 10.1371/journal.pone.0072972. PubMed PMID: 24009723; PubMed Central PMCID: PMCPMC3756947.

34. Lin YL, Wang S. Prenatal lipopolysaccharide exposure increases depression-like behaviors and reduces hippocampal neurogenesis in adult rats. Behav Brain Res. 2014;259:24-34. Epub 2013/11/02. doi: 10.1016/j.bbr.2013.10.034. PubMed PMID: 24177209.

35. Lemaire V, Lamarque S, Le Moal M, Piazza PV, Abrous DN. Postnatal stimulation of the pups counteracts prenatal stress-induced deficits in hippocampal neurogenesis. Biol Psychiatry. 2006;59(9):786-92. Epub 2006/02/08. doi: S0006-3223(05)01400-9 [pii]

10.1016/j.biopsych.2005.11.009. PubMed PMID: 16460692.

36. Weinstock M. Prenatal stressors in rodents: Effects on behavior. Neurobiology of stress. 2017;6:3-13. doi: 10.1016/j.ynstr.2016.08.004. PubMed PMID: 28229104; PubMed Central PMCID: PMCPMC5314420.

37. Glover V. Annual Research Review: Prenatal stress and the origins of psychopathology: an evolutionary perspective. J Child Psychol Psychiatry. 2011;52(4):356-67. Epub 2011/01/22. doi: 10.1111/j.1469-7610.2011.02371.x. PubMed PMID: 21250994.

38. Otis EM, Brent R. Equivalent ages in mouse and human embryos. Anat Rec. 1954;120(1):33-63. Epub 1954/09/01. doi: 10.1002/ar.1091200104. PubMed PMID: 13207763.

39. Fujioka A, Fujioka T, Ishida Y, Maekawa T, Nakamura S. Differential effects of prenatal stress on the morphological maturation of hippocampal neurons. Neuroscience. 2006;141(2):907-15. Epub 2006/06/27. doi: 10.1016/j.neuroscience.2006.04.046. PubMed PMID: 16797130.

40. Tanapat P, Hastings NB, Reeves AJ, Gould E. Estrogen stimulates a transient increase in the number of new neurons in the dentate gyrus of the adult female rat. J Neurosci. 1999;19(14):5792-801. Epub 1999/07/17. PubMed PMID: 10407020; PubMed Central PMCID: PMCPMC6783062.

41. Van den Hove DLA, Kenis G, Brass A, Opstelten R, Rutten BPF, Bruschettini M, et al. Vulnerability versus resilience to prenatal stress in male and female rats; Implications from gene expression profiles in the hippocampus and frontal cortex. European Neuropsychopharmacology. 2013;23(10):1226-46. doi: https://doi.org/10.1016/j.euroneuro.2012.09.011.

42. Nugent BM, O'Donnell CM, Epperson CN, Bale TL. Placental H3K27me3 establishes female resilience to prenatal insults. Nat Commun. 2018;9(1):2555. Epub 2018/07/04. doi: 10.1038/s41467-018-04992-1. PubMed PMID: 29967448; PubMed Central PMCID: PMCPMC6028627.

43. Aleman A, Kahn RS, Selten JP. Sex differences in the risk of schizophrenia: evidence from meta-analysis. Arch Gen Psychiatry. 2003;60(6):565-71. Epub 2003/06/11. doi: 10.1001/archpsyc.60.6.565. PubMed PMID: 12796219.

44. Baron-Cohen S, Knickmeyer RC, Belmonte MK. Sex Differences in the Brain: Implications for Explaining Autism. Science. 2005;310(5749):819-23. doi: doi:10.1126/science.1115455.

45. Kidger AM, Sipthorp J, Cook SJ. ERK1/2 inhibitors: New weapons to inhibit the RAS-regulated RAF-MEK1/2-ERK1/2 pathway. Pharmacol Ther. 2018;187:45-60. Epub 2018/02/20. doi: 10.1016/j.pharmthera.2018.02.007. PubMed PMID: 29454854.

46. Doetsch F, Petreanu L, Caille I, Garcia-Verdugo JM, Alvarez-Buylla A. EGF converts transit-amplifying neurogenic precursors in the adult brain into multipotent stem cells. Neuron. 2002;36(6):1021-34. Epub 2002/12/24. doi: 10.1016/s0896-6273(02)01133-9. PubMed PMID: 12495619.

47. Huang C-Y, Tan T-H. DUSPs, to MAP kinases and beyond. Cell & Bioscience. 2012;2(1):24. doi: 10.1186/2045-3701-2-24.

48. Coskun V, Wu H, Blanchi B, Tsao S, Kim K, Zhao J, et al. CD133+ neural stem cells in the ependyma of mammalian postnatal forebrain. Proc Natl Acad Sci U S A. 2008;105(3):1026-31. Epub 2008/01/16. doi: 10.1073/pnas.0710000105. PubMed PMID: 18195354; PubMed Central PMCID: PMCPMC2242680.

49. Klein SL, Flanagan KL. Sex differences in immune responses. Nature Reviews Immunology. 2016;16(10):626-38. doi: 10.1038/nri.2016.90.

50. Lee C-M, Zhou L, Liu J, Shi J, Geng Y, Liu M, et al. Single-cell RNA-seq analysis revealed long-lasting adverse effects of tamoxifen on neurogenesis in prenatal and adult brains. Proceedings of the National Academy of Sciences. 2020;117(32):19578. doi: 10.1073/pnas.1918883117.

51. Wang G, Wen WX, Mead AJ, Roy A, Psaila B, Thongjuea S. Processing single-cell RNA-seq datasets using SingCellaR. STAR Protoc. 2022;3(2):101266. Epub 2022/04/09. doi: 10.1016/j.xpro.2022.101266. PubMed PMID: 35391938; PubMed Central PMCID: PMCPMC8980964.

52. Roy A, Wang G, Iskander D, O'Byrne S, Elliott N, O'Sullivan J, et al. Transitions in lineage specification and gene regulatory networks in hematopoietic stem/progenitor cells over human development. Cell Rep. 2021;36(11):109698. Epub 2021/09/16. doi: 10.1016/j.celrep.2021.109698. PubMed PMID: 34525349; PubMed Central PMCID: PMCPMC8456780.

53. Martin A, Calvigioni D, Tzortzi O, Fuzik J, Warnberg E, Meletis K. A Spatiomolecular Map of the Striatum. Cell Rep. 2019;29(13):4320-33 e5. Epub 2019/12/26. doi: 10.1016/j.celrep.2019.11.096. PubMed PMID: 31875543.

54. Gokce O, Stanley Geoffrey M, Treutlein B, Neff Norma F, Camp JG, Malenka Robert C, et al. Cellular Taxonomy of the Mouse Striatum as Revealed by Single-Cell RNA-Seq. Cell Reports. 2016;16(4):1126-37. doi: https://doi.org/10.1016/j.celrep.2016.06.059.

55. Zheng SC, Stein-O'Brien G, Augustin JJ, Slosberg J, Carosso GA, Winer B, et al. Universal prediction of cell-cycle position using transfer learning. Genome Biol. 2022;23(1):41. Epub 2022/02/02. doi: 10.1186/s13059-021-02581-y. PubMed PMID: 35101061; PubMed Central PMCID: PMCPMC8802487.

56. Codega P, Silva-Vargas V, Paul A, Maldonado-Soto AR, Deleo AM, Pastrana E, et al. Prospective identification and purification of quiescent adult neural stem cells from their in vivo niche. Neuron. 2014;82(3):545-59. Epub 2014/05/09. doi: 10.1016/j.neuron.2014.02.039. PubMed PMID: 24811379; PubMed Central PMCID: PMCPMC4360885.

57. Inta D, Cameron HA, Gass P. New neurons in the adult striatum: from rodents to humans. Trends Neurosci. 2015;38(9):517-23. Epub 2015/08/25. doi: 10.1016/j.tins.2015.07.005. PubMed PMID: 26298770; PubMed Central PMCID: PMCPMC4564523.

58. Iacono G, Massoni-Badosa R, Heyn H. Single-cell transcriptomics unveils gene regulatory network plasticity. Genome biology. 2019;20(1):110. Epub 2019/06/05. doi: 10.1186/s13059-019-1713-4. PubMed PMID: 31159854; PubMed Central PMCID: PMCPMC6547541.

59. Zou JX, Revenko AS, Li LB, Gemo AT, Chen H-W. ANCCA, an estrogen-regulated AAA+ ATPase coactivator for ERalpha;, is required for coregulator occupancy and chromatin modification. Proceedings of the National Academy of Sciences. 2007;104(46):18067-72. doi: doi:10.1073/pnas.0705814104.

60. Murakami S, Li R, Nagari A, Chae M, Camacho CV, Kraus WL. Distinct Roles for BET Family Members in Estrogen Receptor α Enhancer Function and Gene Regulation in Breast Cancer Cells. Mol Cancer Res. 2019;17(12):2356-68. Epub 2019/09/26. doi: 10.1158/1541-7786.Mcr-19-0393. PubMed PMID: 31551256; PubMed Central PMCID: PMCPMC6891197.

61. Browne JA, NandyMazumdar M, Paranjapye A, Leir SH, Harris A. The Bromodomain Containing 8 (BRD8) transcriptional network in human lung epithelial cells. Mol Cell Endocrinol. 2021;524:111169. Epub 2021/01/22. doi: 10.1016/j.mce.2021.111169. PubMed PMID: 33476703; PubMed Central PMCID: PMCPMC8035426.

62. Leung HW, Leung CON, Lau EY, Chung KPS, Mok EH, Lei MML, et al. EPHB2 Activates β-Catenin to Enhance Cancer Stem Cell Properties and Drive Sorafenib Resistance in Hepatocellular Carcinoma. Cancer Res. 2021;81(12):3229-40. Epub 2021/04/28. doi: 10.1158/0008-5472.Can-21-0184. PubMed PMID: 33903122.

63. Shah M, Rennoll SA, Raup-Konsavage WM, Yochum GS. A dynamic exchange of TCF3 and TCF4 transcription factors controls MYC expression in colorectal cancer cells. Cell Cycle. 2015;14(3):323-32. Epub 2015/02/07. doi: 10.4161/15384101.2014.980643. PubMed PMID: 25659031; PubMed Central PMCID: PMCPMC4353228.

64. Pereira JD, Sansom SN, Smith J, Dobenecker MW, Tarakhovsky A, Livesey FJ. Ezh2, the histone methyltransferase of PRC2, regulates the balance between self-renewal and differentiation in the cerebral cortex.

Proc Natl Acad Sci U S A. 2010;107(36):15957-62. Epub 2010/08/28. doi: 10.1073/pnas.1002530107. PubMed PMID: 20798045; PubMed Central PMCID: PMCPMC2936600.

65. Lee KE, Seo J, Shin J, Ji EH, Roh J, Kim JY, et al. Positive feedback loop between Sox2 and Sox6 inhibits neuronal differentiation in the developing central nervous system. Proc Natl Acad Sci U S A. 2014;111(7):2794-9. Epub 2014/02/07. doi: 10.1073/pnas.1308758111. PubMed PMID: 24501124; PubMed Central PMCID: PMCPMC3932859.

66. Li L, Medina-Menendez C, Garcia-Corzo L, Cordoba-Beldad CM, Quiroga AC, Calleja Barca E, et al. SoxD genes are required for adult neural stem cell activation. Cell Rep. 2022;38(5):110313. Epub 2022/02/03. doi: 10.1016/j.celrep.2022.110313. PubMed PMID: 35108528.

67. Jeong WJ, Ro EJ, Choi KY. Interaction between Wnt/beta-catenin and RAS-ERK pathways and an anti-cancer strategy via degradations of beta-catenin and RAS by targeting the Wnt/beta-catenin pathway. NPJ Precis Oncol. 2018;2(1):5. Epub 2018/06/07. doi: 10.1038/s41698-018-0049-y. PubMed PMID: 29872723; PubMed Central PMCID: PMCPMC5871897.

68. Improta-Brears T, Whorton AR, Codazzi F, York JD, Meyer T, McDonnell DP. Estrogen-induced activation of mitogen-activated protein kinase requires mobilization of intracellular calcium. Proceedings of the National Academy of Sciences. 1999;96(8):4686-91. doi: doi:10.1073/pnas.96.8.4686.

69. Satoh Y, Kobayashi Y, Takeuchi A, Pagès G, Pouysségur J, Kazama T. Deletion of ERK1 and ERK2 in the CNS causes cortical abnormalities and neonatal lethality: Erk1 deficiency enhances the impairment of neurogenesis in Erk2-deficient mice. J Neurosci. 2011;31(3):1149-55. Epub 2011/01/21. doi: 10.1523/jneurosci.2243-10.2011. PubMed PMID: 21248139; PubMed Central PMCID: PMCPMC6632941.

70. Vithayathil J, Pucilowska J, Goodnough LH, Atit RP, Landreth GE. Dentate Gyrus Development Requires ERK Activity to Maintain Progenitor Population and MAPK Pathway Feedback Regulation. J Neurosci. 2015;35(17):6836-48. Epub 2015/05/01. doi: 10.1523/jneurosci.4196-14.2015. PubMed PMID: 25926459; PubMed Central PMCID: PMCPMC4412899.

71. Shi Z, Geng Y, Liu J, Zhang H, Zhou L, Lin Q, et al. Single-cell transcriptomics reveals gene signatures and alterations associated with aging in distinct neural stem/progenitor cell subpopulations. Protein Cell. 2018;9(4):351-64. Epub 2017/07/28. doi: 10.1007/s13238-017-0450-2. PubMed PMID: 28748452; PubMed Central PMCID: PMCPMC5876182.

72. Morshead CM, Reynolds BA, Craig CG, McBurney MW, Staines WA, Morassutti D, et al. Neural stem cells in the adult mammalian forebrain: a relatively quiescent subpopulation of subependymal cells. Neuron. 1994;13(5):1071-82. Epub 1994/11/01. doi: 10.1016/0896-6273(94)90046-9. PubMed PMID: 7946346.

73. Llorens-Bobadilla E, Zhao S, Baser A, Saiz-Castro G, Zwadlo K, Martin-Villalba A. Single-Cell Transcriptomics Reveals a Population of Dormant Neural Stem Cells that Become Activated upon Brain Injury. Cell Stem Cell. 2015;17(3):329-40. doi: https://doi.org/10.1016/j.stem.2015.07.002.

74. Boldrini M, Fulmore CA, Tartt AN, Simeon LR, Pavlova I, Poposka V, et al. Human Hippocampal Neurogenesis Persists throughout Aging. Cell Stem Cell. 2018;22(4):589-99 e5. Epub 2018/04/07. doi: 10.1016/j.stem.2018.03.015. PubMed PMID: 29625071; PubMed Central PMCID: PMCPMC5957089.

75. Durante MA, Kurtenbach S, Sargi ZB, Harbour JW, Choi R, Kurtenbach S, et al. Single-cell analysis of olfactory neurogenesis and differentiation in adult humans. Nat Neurosci. 2020;23(3):323-6. Epub 2020/02/19. doi: 10.1038/s41593-020-0587-9. PubMed PMID: 32066986; PubMed Central PMCID: PMCPMC7065961.

76. Eriksson PS, Perfilieva E, Björk-Eriksson T, Alborn A-M, Nordborg C, Peterson DA, et al. Neurogenesis in the adult human hippocampus. Nature Medicine. 1998;4(11):1313-7. doi: 10.1038/3305.

77. Franjic D, Skarica M, Ma S, Arellano JI, Tebbenkamp ATN, Choi J, et al. Transcriptomic taxonomy and neurogenic trajectories of adult human, macaque, and pig hippocampal and entorhinal cells. Neuron. 2022;110(3):452-69.e14. Epub 2021/11/20. doi: 10.1016/j.neuron.2021.10.036. PubMed PMID: 34798047; PubMed Central PMCID: PMCPMC8813897.

78. Gotz M, Huttner WB. The cell biology of neurogenesis. Nat Rev Mol Cell Biol. 2005;6(10):777-88. Epub 2005/11/30. doi: 10.1038/nrm1739. PubMed PMID: 16314867.

79. Denoth-Lippuner A, Jessberger S. Formation and integration of new neurons in the adult hippocampus. Nat Rev Neurosci. 2021;22(4):223-36. Epub 2021/02/27. doi: 10.1038/s41583-021-00433-z. PubMed PMID: 33633402.

80. Fuentealba LC, Obernier K, Alvarez-Buylla A. Adult neural stem cells bridge their niche. Cell stem cell. 2012;10(6):698-708. doi: 10.1016/j.stem.2012.05.012. PubMed PMID: 22704510.

81. Deryckere A, Stappers E, Dries R, Peyre E, van den Berghe V, Conidi A, et al. Multifaceted actions of Zeb2 in postnatal neurogenesis from the ventricular-subventricular zone to the olfactory bulb. Development. 2020;147(10). Epub 2020/04/08. doi: 10.1242/dev.184861. PubMed PMID: 32253238.

82. Fardi M, Alivand M, Baradaran B, Farshdousti Hagh M, Solali S. The crucial role of ZEB2: From development to epithelial-to-mesenchymal transition and cancer complexity. J Cell Physiol. 2019. Epub 2019/02/19. doi: 10.1002/jcp.28277. PubMed PMID: 30773635.

83. Dongre A, Weinberg RA. New insights into the mechanisms of epithelial–mesenchymal transition and implications for cancer. Nature Reviews Molecular Cell Biology. 2019;20(2):69-84. doi: 10.1038/s41580-018-0080-4.

84. Birkhoff JC, Brouwer RWW, Kolovos P, Korporaal AL, Bermejo-Santos A, Boltsis I, et al. Targeted chromatin conformation analysis identifies novel distal neural enhancers of ZEB2 in pluripotent stem cell differentiation. Hum Mol Genet. 2020;29(15):2535-50. Epub 2020/07/07. doi: 10.1093/hmg/ddaa141. PubMed PMID: 32628253; PubMed Central PMCID: PMCPMC7471508.

85. Miquelajauregui A, Van de Putte T, Polyakov A, Nityanandam A, Boppana S, Seuntjens E, et al. Smad-interacting protein-1 (Zfhx1b) acts upstream of Wnt signaling in the mouse hippocampus and controls its formation. Proc Natl Acad Sci U S A. 2007;104(31):12919-24. Epub 2007/07/24. doi: 10.1073/pnas.0609863104. PubMed PMID: 17644613; PubMed Central PMCID: PMCPMC1929013.

86. Hardy D, Malvaut S, Breton-Provencher V, Saghatelyan A. The role of calretinin-expressing granule cells in olfactory bulb functions and odor behavior. Sci Rep. 2018;8(1):9385. Epub 2018/06/22. doi: 10.1038/s41598-018-27692-8. PubMed PMID: 29925844; PubMed Central PMCID: PMCPMC6010413.

87. Das S, Sadanandappa MK, Dervan A, Larkin A, Lee JA, Sudhakaran IP, et al. Plasticity of local GABAergic interneurons drives olfactory habituation. Proc Natl Acad Sci U S A. 2011;108(36):E646-54. Epub 2011/07/29. doi: 10.1073/pnas.1106411108. PubMed PMID: 21795607; PubMed Central PMCID: PMCPMC3169145.

88. Heinbockel T, Laaris N, Ennis M. Metabotropic glutamate receptors in the main olfactory bulb drive granule cell-mediated inhibition. J Neurophysiol. 2007;97(1):858-70. Epub 2006/11/10. doi: 10.1152/jn.00884.2006. PubMed PMID: 17093122; PubMed Central PMCID: PMCPMC2788779.

89. Nunes D, Kuner T. Disinhibition of olfactory bulb granule cells accelerates odour discrimination in mice. Nature Communications. 2015;6(1):8950. doi: 10.1038/ncomms9950.

90. Alonso M, Viollet C, Gabellec MM, Meas-Yedid V, Olivo-Marin JC, Lledo PM. Olfactory discrimination learning increases the survival of adult-born neurons in the olfactory bulb. J Neurosci. 2006;26(41):10508-13. Epub 2006/10/13. doi: 10.1523/jneurosci.2633-06.2006. PubMed PMID: 17035535; PubMed Central PMCID: PMCPMC6674694.

91. Breton-Provencher V, Lemasson M, Peralta MR, 3rd, Saghatelyan A. Interneurons produced in adulthood are required for the normal functioning of the olfactory bulb network and for the execution of selected olfactory behaviors. J Neurosci. 2009;29(48):15245-57. Epub 2009/12/04. doi: 10.1523/JNEUROSCI.3606-09.2009. PubMed PMID: 19955377; PubMed Central PMCID: PMCPMC6665973.

92. Moreno MM, Linster C, Escanilla O, Sacquet J, Didier A, Mandairon N. Olfactory perceptual learning requires adult neurogenesis. Proc Natl Acad Sci U S A. 2009;106(42):17980-5. Epub 2009/10/10. doi: 10.1073/pnas.0907063106. PubMed PMID: 19815505; PubMed Central PMCID: PMCPMC2764902.

93. Whitman MC, Greer CA. Adult neurogenesis and the olfactory system. Prog Neurobiol. 2009;89(2):162-75. Epub 2009/07/21. doi: 10.1016/j.pneurobio.2009.07.003. PubMed PMID: 19615423; PubMed Central PMCID: PMCPMC2748178.

94. Yang M, Crawley JN. Simple behavioral assessment of mouse olfaction. Curr Protoc Neurosci. 2009;Chapter 8:Unit 8 24. Epub 2009/07/04. doi: 10.1002/0471142301.ns0824s48. PubMed PMID: 19575474; PubMed Central PMCID: PMCPMC2753229.

95. Love MI, Huber W, Anders S. Moderated estimation of fold change and dispersion for RNA-seq data with DESeq2. Genome Biol. 2014;15(12):550. Epub 2014/12/18. doi: 10.1186/s13059-014-0550-8. PubMed PMID: 25516281; PubMed Central PMCID: PMCPMC4302049.

96. Langfelder P, Horvath S. WGCNA: an R package for weighted correlation network analysis. BMC Bioinformatics. 2008;9:559. Epub 2008/12/31. doi: 10.1186/1471-2105-9-559. PubMed PMID: 19114008; PubMed Central PMCID: PMCPMC2631488.

97. Wu T, Hu E, Xu S, Chen M, Guo P, Dai Z, et al. clusterProfiler 4.0: A universal enrichment tool for interpreting omics data. Innovation (Camb). 2021;2(3):100141. Epub 2021/09/25. doi: 10.1016/j.xinn.2021.100141. PubMed PMID: 34557778; PubMed Central PMCID: PMCPMC8454663.

98. Hu P, Fabyanic E, Kwon DY, Tang S, Zhou Z, Wu H. Dissecting Cell-Type Composition and Activity-Dependent Transcriptional State in Mammalian Brains by Massively Parallel Single-Nucleus RNA-Seq. Mol Cell. 2017;68(5):1006-15 e7. Epub 2017/12/09. doi: 10.1016/j.molcel.2017.11.017. PubMed PMID: 29220646; PubMed Central PMCID: PMCPMC5743496.

Figure 1

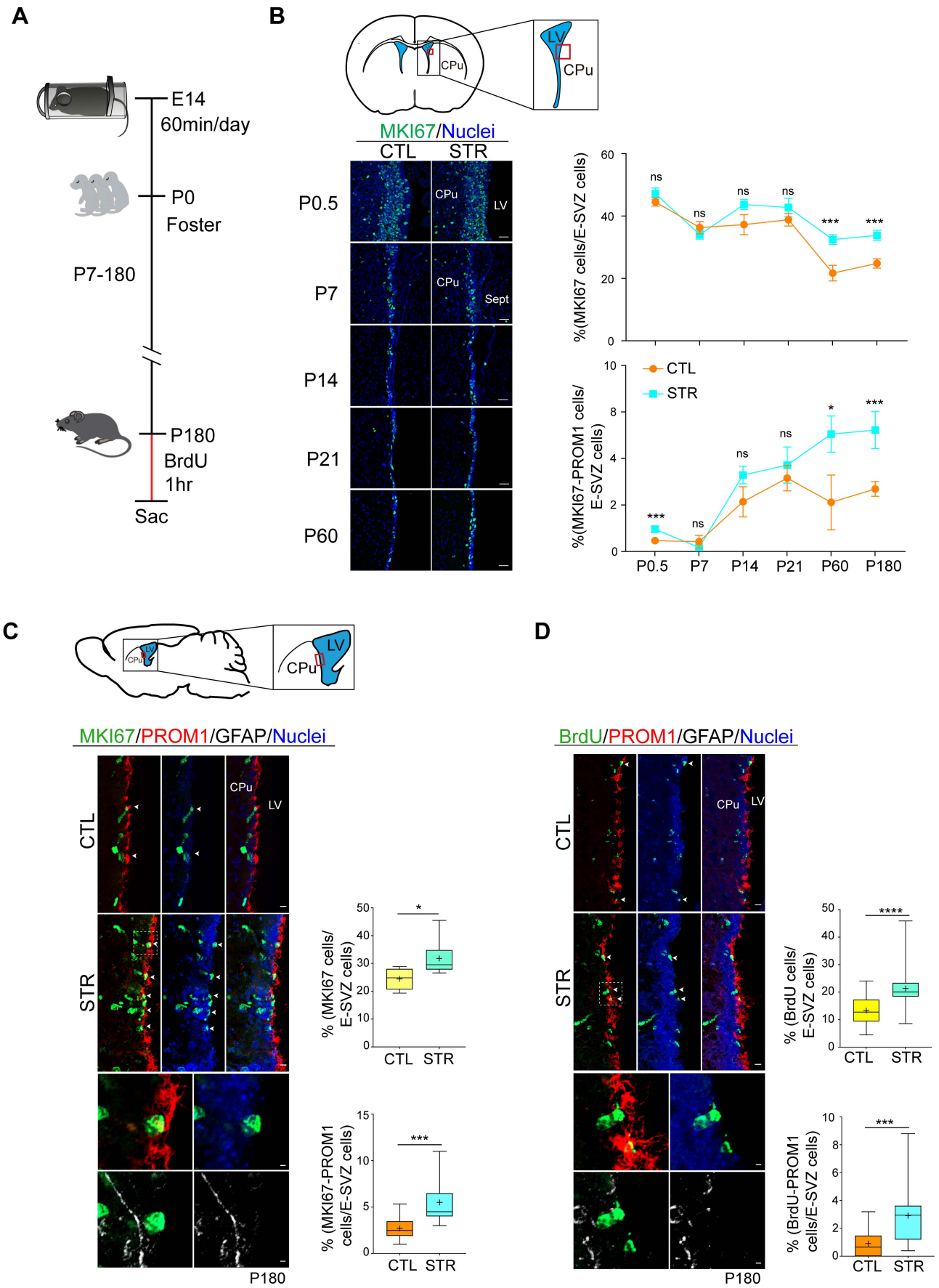
A
E14
60min/day
P0
Foster
P7-180
P180
BrdU
1hr
Sac
B
LV
CPu
MKI67/Nuclei
CTL
STR
P0.5
P7
P14
P21
P60
Sept
%(MKI67 cells/E-SVZ cells)
%(MKI67-PROM1 cells/ E-SVZ cells)
CTL
STR
ns
***
*
P0.5
P7
P14
P21
P60
P180
C
MKI67/PROM1/GFAP/Nuclei
CTL
STR
% (MKI67 cells/ E-SVZ cells)
% (MKI67-PROM1 cells/E-SVZ cells)
P180
D
BrdU/PROM1/GFAP/Nuclei
% (BrdU cells/ E-SVZ cells)
% (BrdU-PROM1 cells/E-SVZ cells)
****

Figure 2

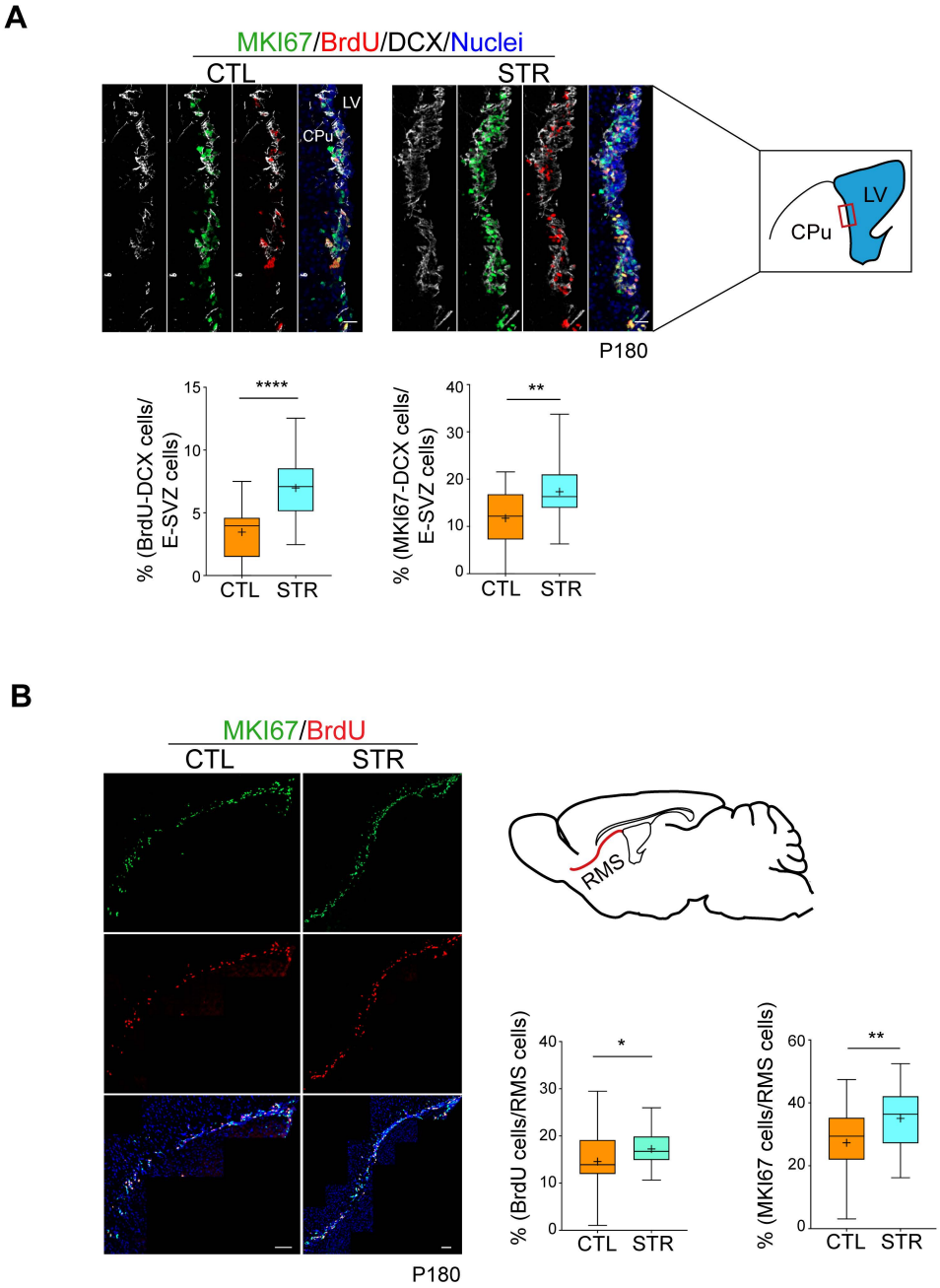
A
MKI67/BrdU/DCX/Nuclei
CTL
STR
LV
CPu
P180
% (BrdU-DCX cells/ E-SVZ cells)
****
CTL
STR
% (MKI67-DCX cells/ E-SVZ cells)
**
B
MKI67/BrdU
RMS
% (BrdU cells/RMS cells)
*
% (MKI67 cells/RMS cells)
**

Figure 3

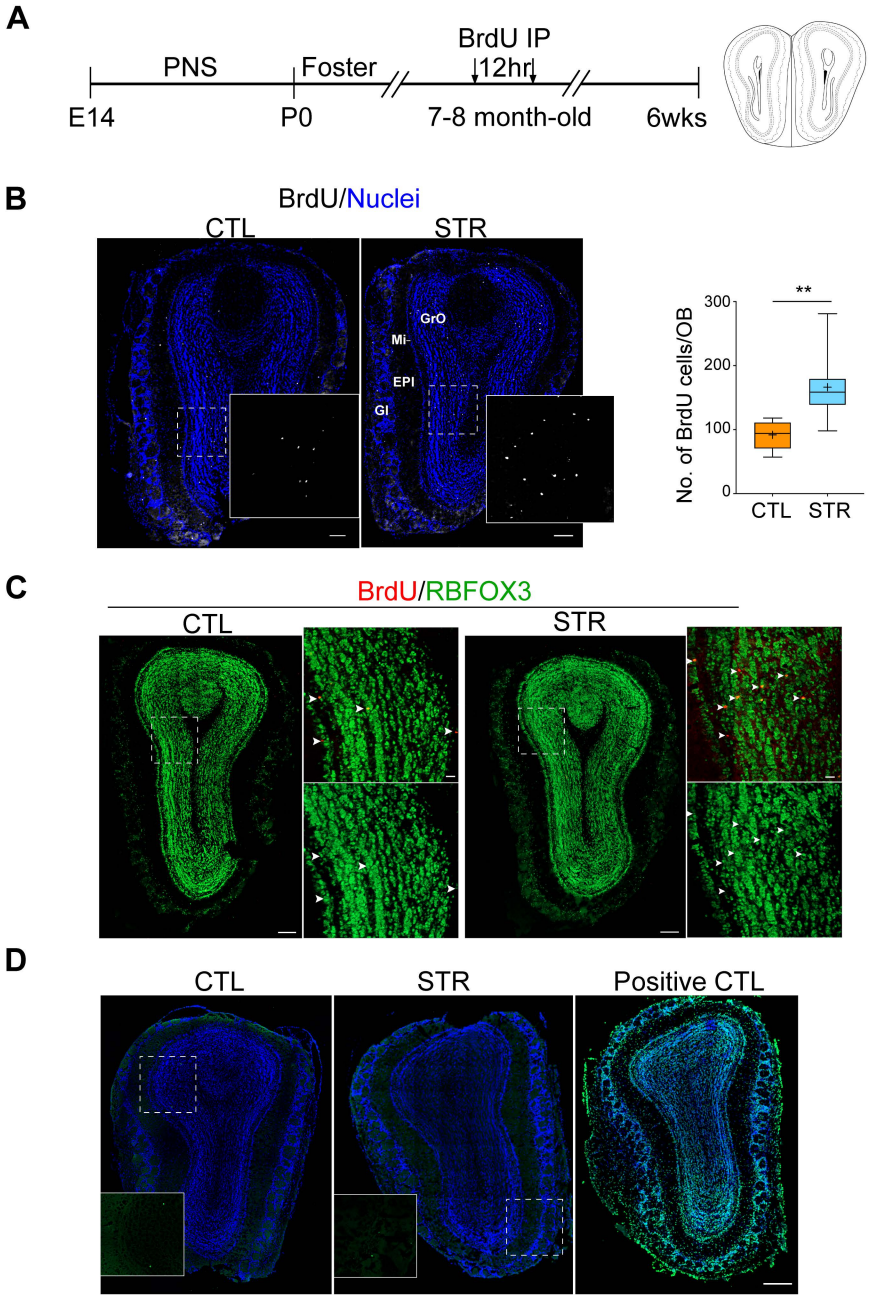
A
PNS
Foster
BrdU IP
12hr
E14
P0
7-8 month-old
6wks
B
BrdU/Nuclei
CTL
STR
GrO
Mi-
EPI
GI
No. of BrdU cells/OB
300
200
100
0
**
CTL
STR
C
BrdU/RBFOX3
CTL
STR
D
CTL
STR
Positive CTL

Figure 4

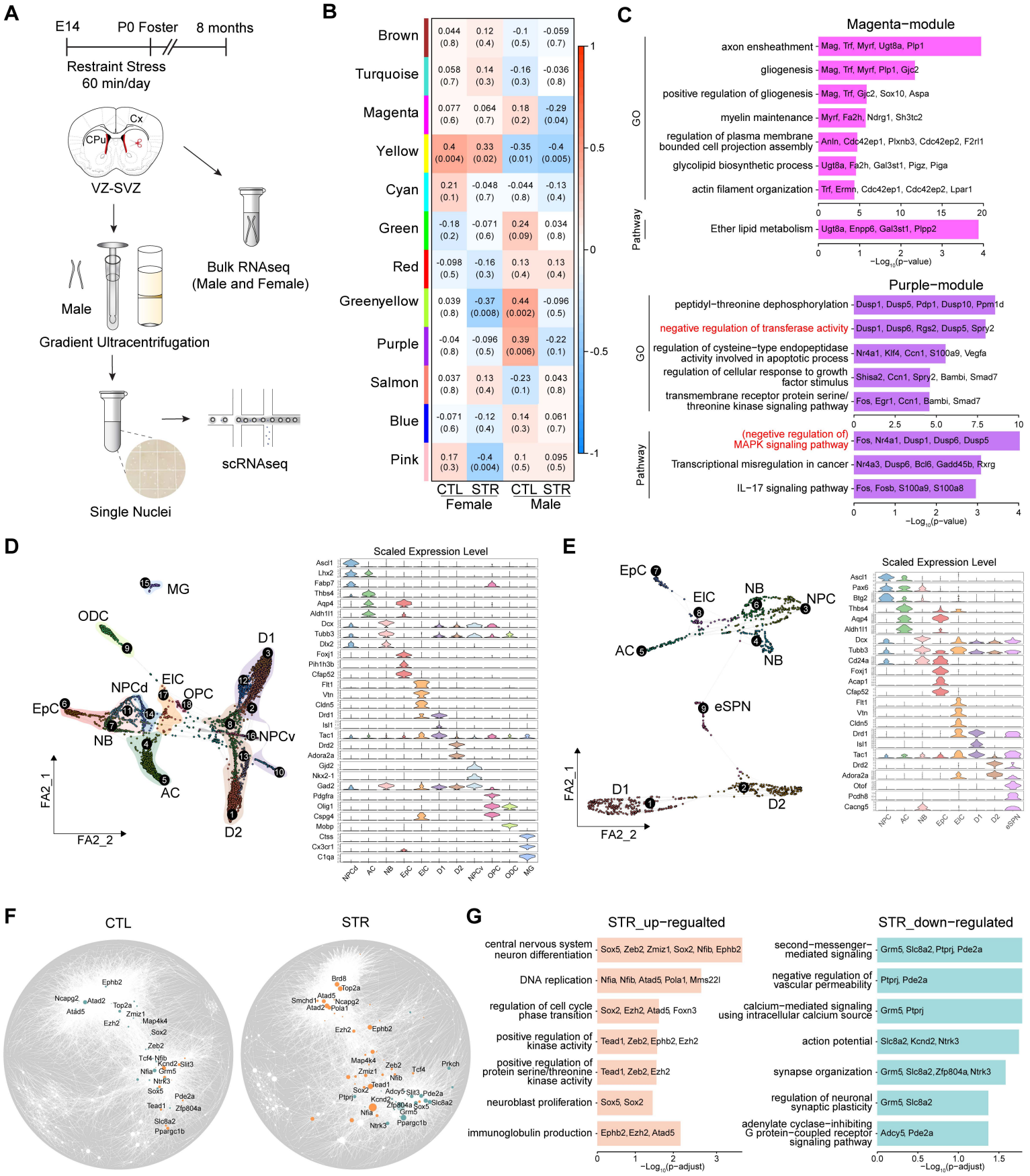
A
E14
P0 Foster
8 months
Restraint Stress
60 min/day
Cx
CPu
VZ-SVZ
Bulk RNAseq
(Male and Female)
Male
Gradient Ultracentrifugation
scRNAseq
Single Nuclei
B
Brown
Turquoise
Magenta
Yellow
Cyan
Green
Red
Greenyellow
Purple
Salmon
Blue
Pink
CTL STR CTL STR
Female Male
C
Magenta−module
GO
Pathway
axon ensheathment - Mag, Trf, Myrf, Ugt8a, Plp1
gliogenesis - Mag, Trf, Myrf, Plp1, Gjc2
positive regulation of gliogenesis - Mag, Trf, Gjc2, Sox10, Aspa
myelin maintenance - Myrf, Fa2h, Ndrg1, Sh3tc2
regulation of plasma membrane bounded cell projection assembly - Anln, Cdc42ep1, Plxnb3, Cdc42ep2, F2rl1
glycolipid biosynthetic process - Ugt8a, Fa2h, Gal3st1, Pigz, Piga
actin filament organization - Trf, Ermn, Cdc42ep1, Cdc42ep2, Lpar1
Ether lipid metabolism - Ugt8a, Enpp6, Gal3st1, Plpp2
−Log10(p−value)
Purple−module
peptidyl−threonine dephosphorylation - Dusp1, Dusp5, Pdp1, Dusp10, Ppm1d
negative regulation of transferase activity - Dusp1, Dusp6, Rgs2, Dusp5, Spry2
regulation of cysteine−type endopeptidase activity involved in apoptotic process - Nr4a1, Klf4, Ccn1, S100a9, Vegfa
regulation of cellular response to growth factor stimulus - Shisa2, Ccn1, Spry2, Bambi, Smad7
transmembrane receptor protein serine/threonine kinase signaling pathway - Fos, Egr1, Ccn1, Bambi, Smad7
(negetive regulation of) MAPK signaling pathway - Fos, Nr4a1, Dusp1, Dusp6, Dusp5
Transcriptional misregulation in cancer - Nr4a3, Dusp6, Bcl6, Gadd45b, Rxrg
IL−17 signaling pathway - Fos, Fosb, S100a9, S100a8
−Log10(p−value)
D
MG
ODC
D1
EIC
NPCd
OPC
EpC
NB
NPCv
AC
D2
FA2_1
FA2_2
Scaled Expression Level
NPCd AC NB EpC EIC D1 D2 NPCv OPC ODC MG
E
EpC
EIC
NB
NPC
AC
NB
eSPN
D1
D2
FA2_1
FA2_2
Scaled Expression Level
NPC AC NB EpC EIC D1 D2 eSPN
F
CTL
STR
G
STR_up−regualted
central nervous system neuron differentiation - Sox5, Zeb2, Zmiz1, Sox2, Nfib, Ephb2
DNA replication - Nfia, Nfib, Atad5, Pola1, Mms22l
regulation of cell cycle phase transition - Sox2, Ezh2, Atad5, Foxn3
positive regulation of kinase activity - Tead1, Zeb2, Ephb2, Ezh2
positive regulation of protein serine/threonine kinase activity - Tead1, Zeb2, Ezh2
neuroblast proliferation - Sox5, Sox2
immunoglobulin production - Ephb2, Ezh2, Atad5
−Log10(p−adjust)
STR_down−regulated
second−messenger−mediated signaling - Grm5, Slc8a2, Ptprj, Pde2a
negative regulation of vascular permeability - Ptprj, Pde2a
calcium−mediated signaling using intracellular calcium source - Grm5, Ptprj
action potential - Slc8a2, Kcnd2, Ntrk3
synapse organization - Grm5, Slc8a2, Zfp804a, Ntrk3
regulation of neuronal synaptic plasticity - Grm5, Slc8a2
adenylate cyclase−inhibiting G protein−coupled receptor signaling pathway - Adcy5, Pde2a
−Log10(p−adjust)

Figure 5

A

Male

p-MAPK3/1/Nuclei

p-MAPK3/1/Nuclei

P0.5 CPu LV CTL STR

P21

P7 CPu Sept CTL STR

P60

P14 CTL STR

P180

B

Male

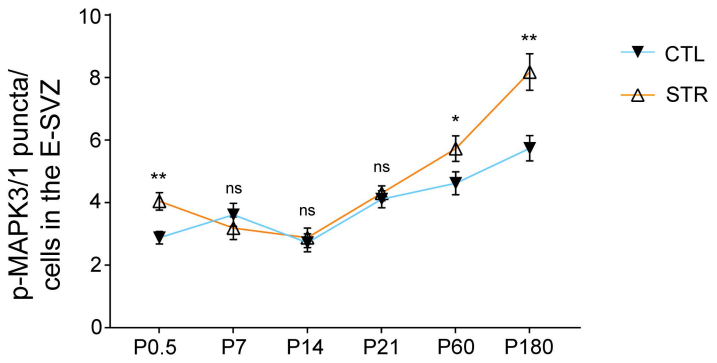

Figure 6

A

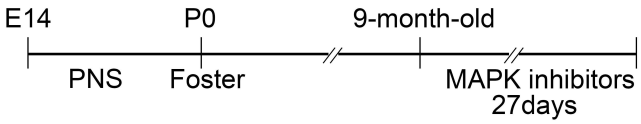
E14
P0
9-month-old
PNS
Foster
MAPK inhibitors
27days

B

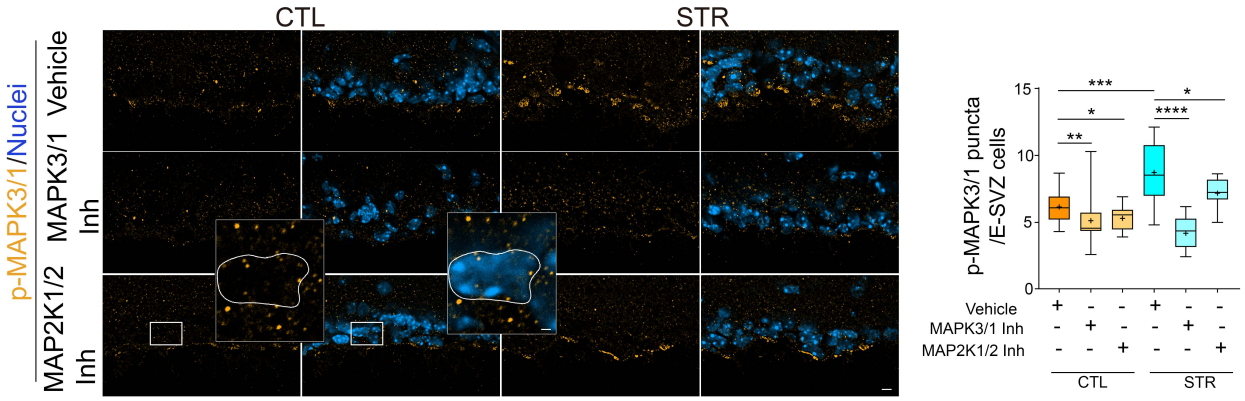
CTL
STR
p-MAPK3/1/Nuclei
Vehicle
MAPK3/1 Inh
MAP2K1/2 Inh
p-MAPK3/1 puncta /E-SVZ cells
Vehicle
MAPK3/1 Inh
MAP2K1/2 Inh
CTL
STR

C

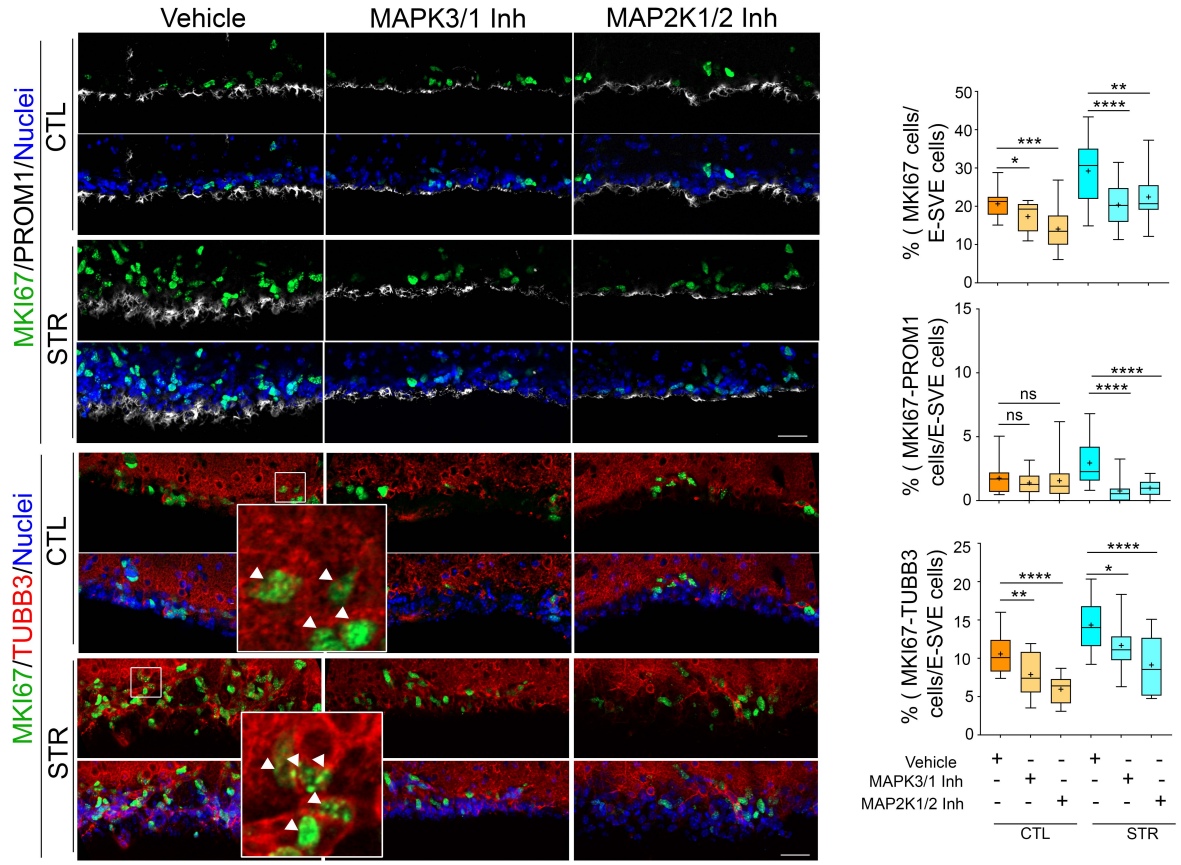
Vehicle
MAPK3/1 Inh
MAP2K1/2 Inh
MKI67/PROM1/Nuclei
CTL
STR
MKI67/TUBB3/Nuclei
CTL
STR
% (MKI67 cells/ E-SVE cells)
% (MKI67-PROM1 cells/E-SVE cells)
% (MKI67-TUBB3 cells/E-SVE cells)
ns
Vehicle
MAPK3/1 Inh
MAP2K1/2 Inh
CTL
STR

Sup. Figure 1

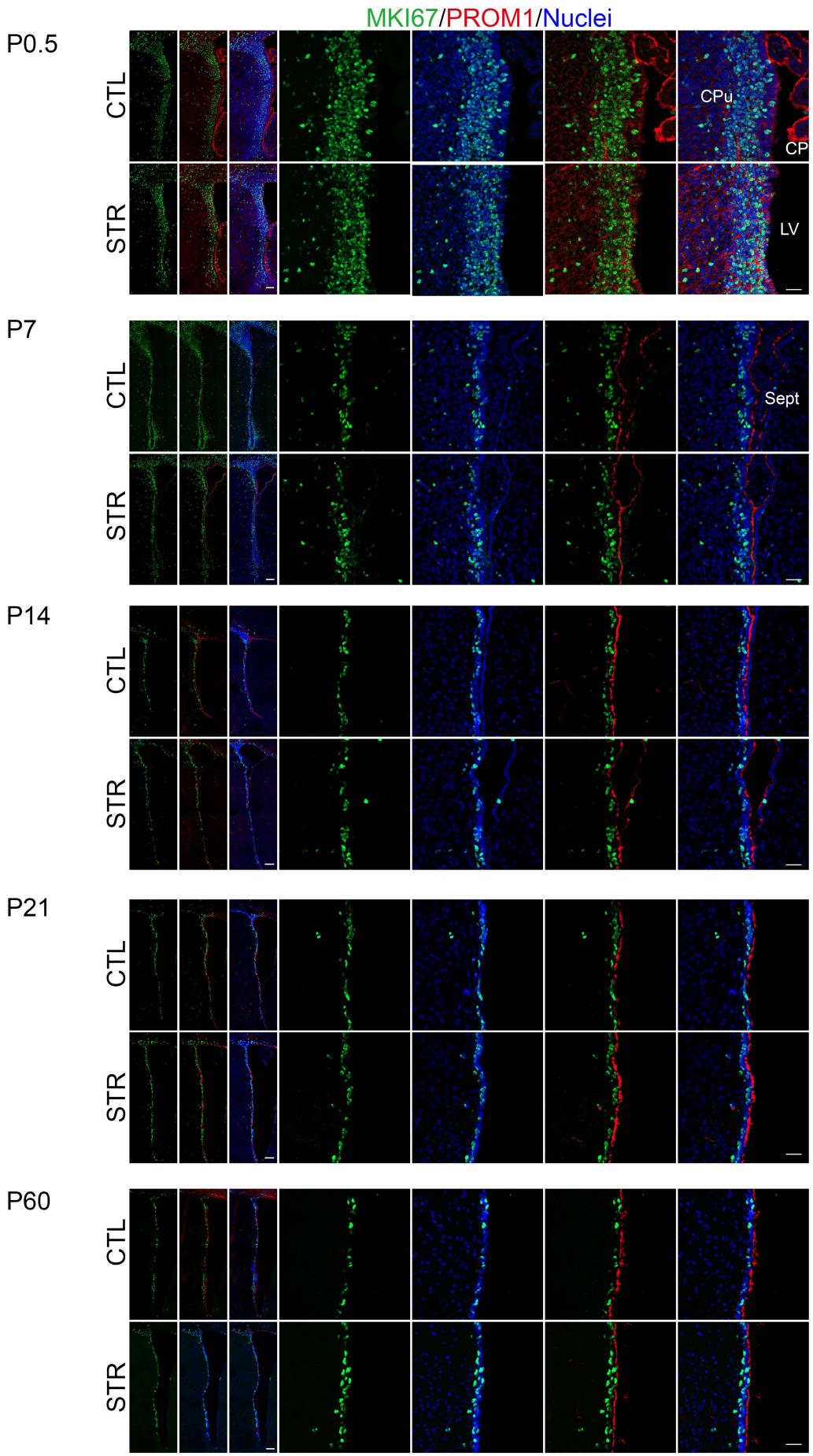
MKI67/PROM1/Nuclei
P0.5
CTL
STR
CPu
CP
LV
P7
CTL
STR
Sept
P14
CTL
STR
P21
CTL
STR
P60
CTL
STR

A

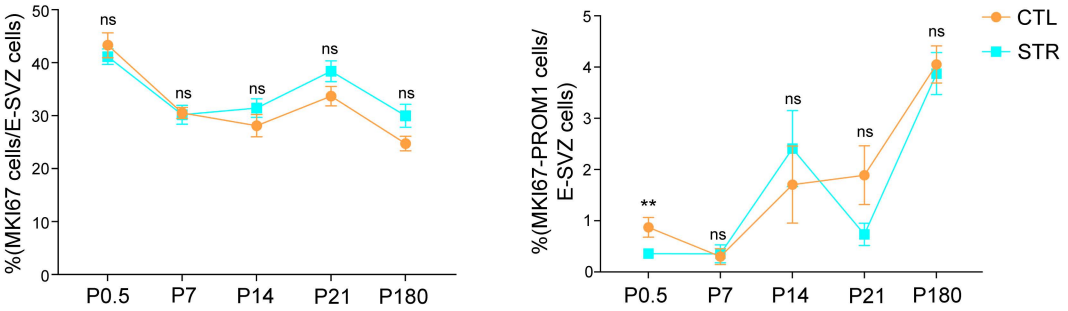
%(MKI67 cells/E-SVZ cells)
50
40
30
20
10
0
ns
ns
ns
ns
ns
P0.5
P7
P14
P21
P180
%(MKI67-PROM1 cells/ E-SVZ cells)
5
4
3
2
1
0
**
ns
ns
ns
ns
P0.5
P7
P14
P21
P180
CTL
STR

B

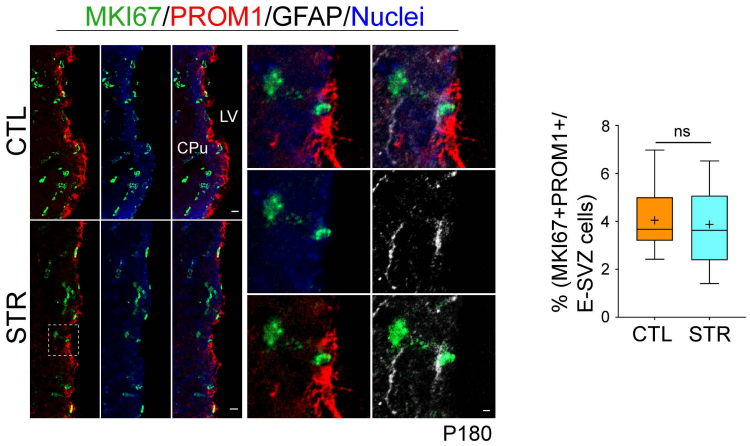
MKI67/PROM1/GFAP/Nuclei
CTL
STR
LV
CPu
P180
% (MKI67+PROM1+/ E-SVZ cells)
8
6
4
2
0
ns
CTL
STR

C

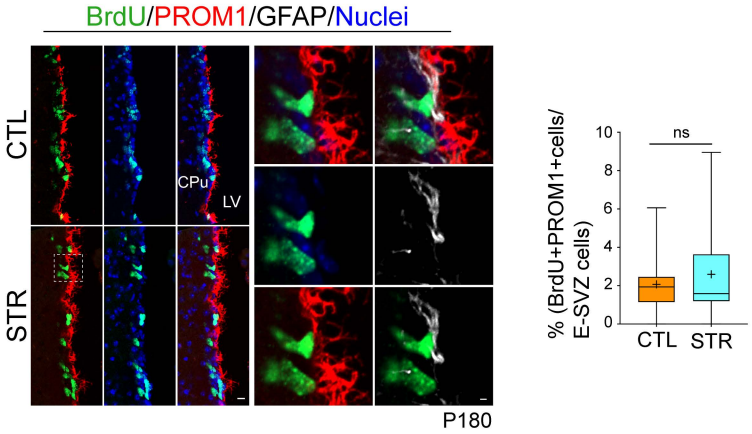
BrdU/PROM1/GFAP/Nuclei
CTL
STR
CPu
LV
P180
% (BrdU+PROM1+cells/ E-SVZ cells)
10
8
6
4
2
0
ns
CTL
STR

D

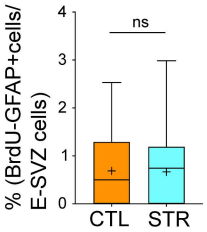
% (BrdU-GFAP+cells/ E-SVZ cells)
4
3
2
1
0
ns
CTL
STR

A

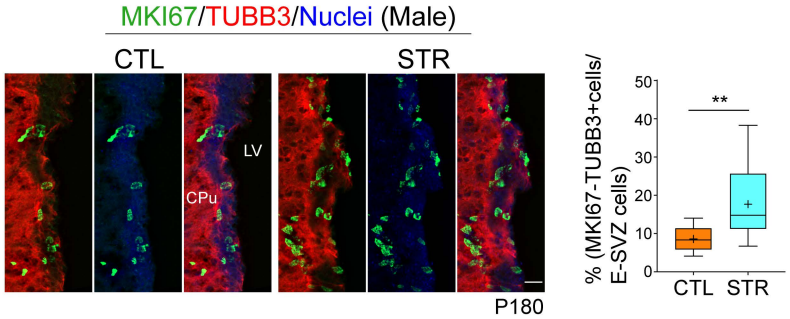
MKI67/TUBB3/Nuclei (Male)
CTL
STR
LV
CPu
P180
% (MKI67-TUBB3+cells/ E-SVZ cells)
50
40
30
20
10
0
**
CTL
STR

B

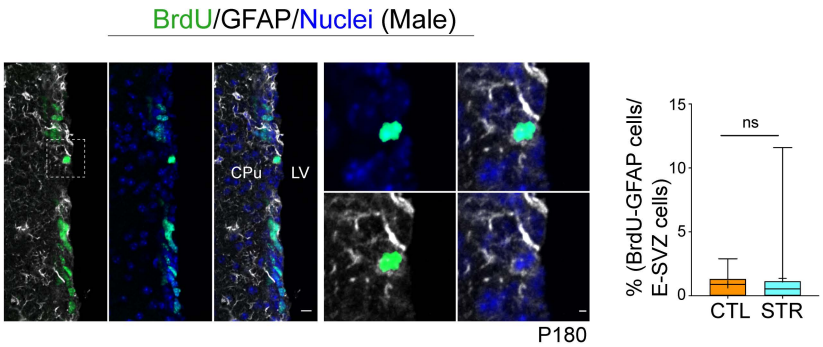
BrdU/GFAP/Nuclei (Male)
CPu
LV
P180
% (BrdU-GFAP cells/ E-SVZ cells)
15
10
5
0
ns
CTL
STR

C

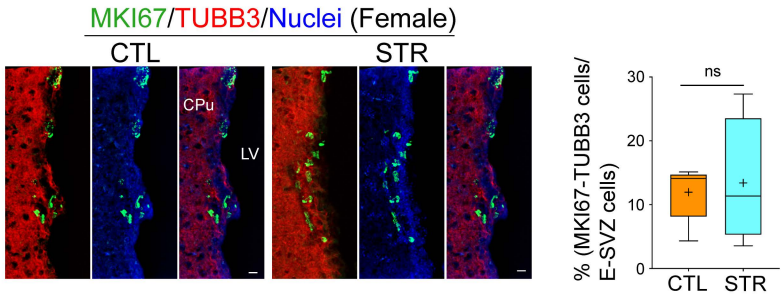
MKI67/TUBB3/Nuclei (Female)
CTL
STR
CPu
LV
% (MKI67-TUBB3 cells/ E-SVZ cells)
30
20
10
0
ns
CTL
STR

D

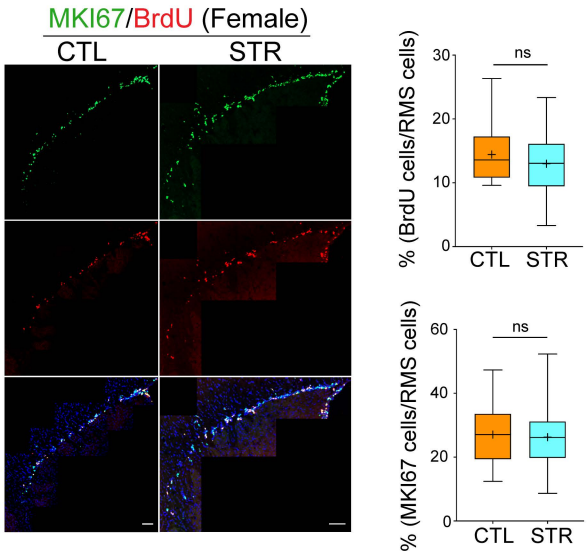
MKI67/BrdU (Female)
CTL
STR
% (BrdU cells/RMS cells)
30
20
10
0
ns
CTL
STR
% (MKI67 cells/RMS cells)
60
40
20
0
ns
CTL
STR

A

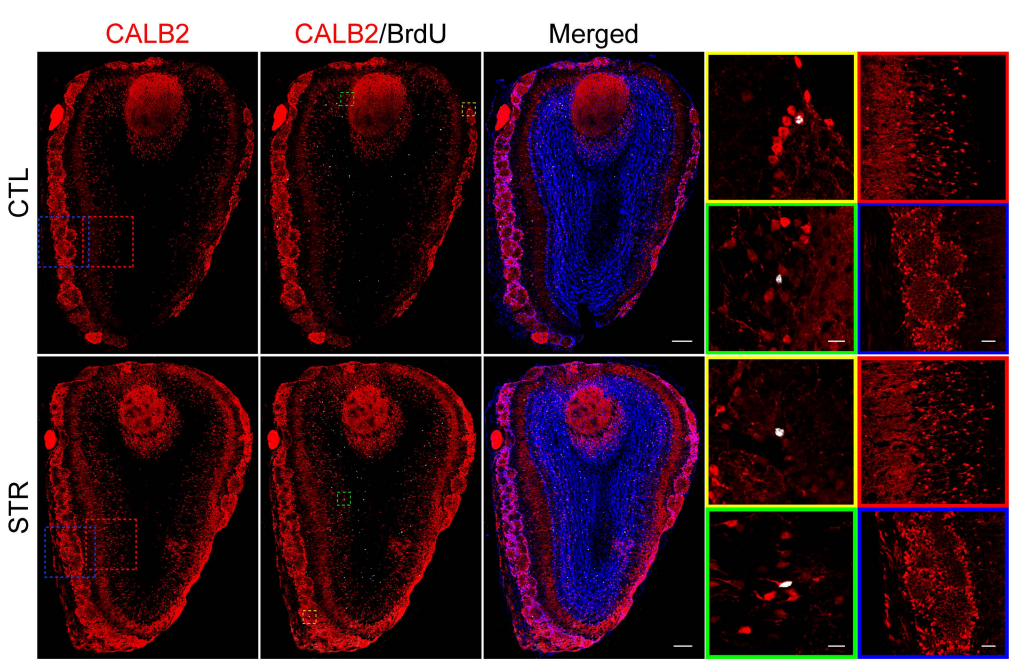
CALB2
CALB2/BrdU
Merged
CTL
STR

B

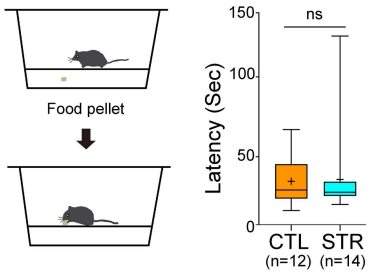
Food pellet
ns
Latency (Sec)
150
100
50
0
CTL
(n=12)
STR
(n=14)

C

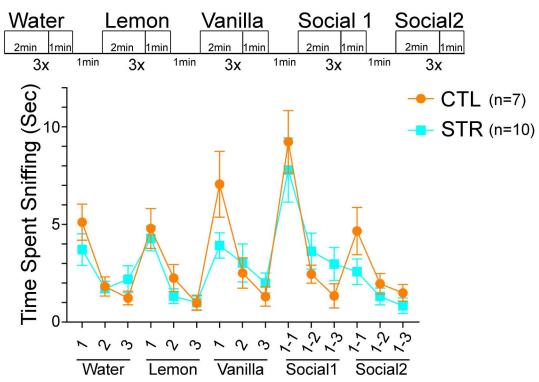
Water
Lemon
Vanilla
Social 1
Social2
2min
1min
3x
CTL (n=7)
STR (n=10)
Time Spent Sniffing (Sec)
10
5
0
Water
Lemon
Vanilla
Social1
Social2

D

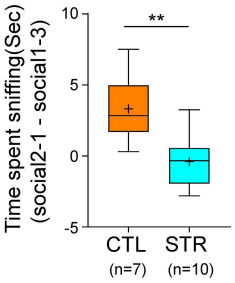
Time spent sniffing(Sec)
(social2-1 - social1-3)
**
10
5
0
-5
CTL
(n=7)
STR
(n=10)

Sup. Figure 5

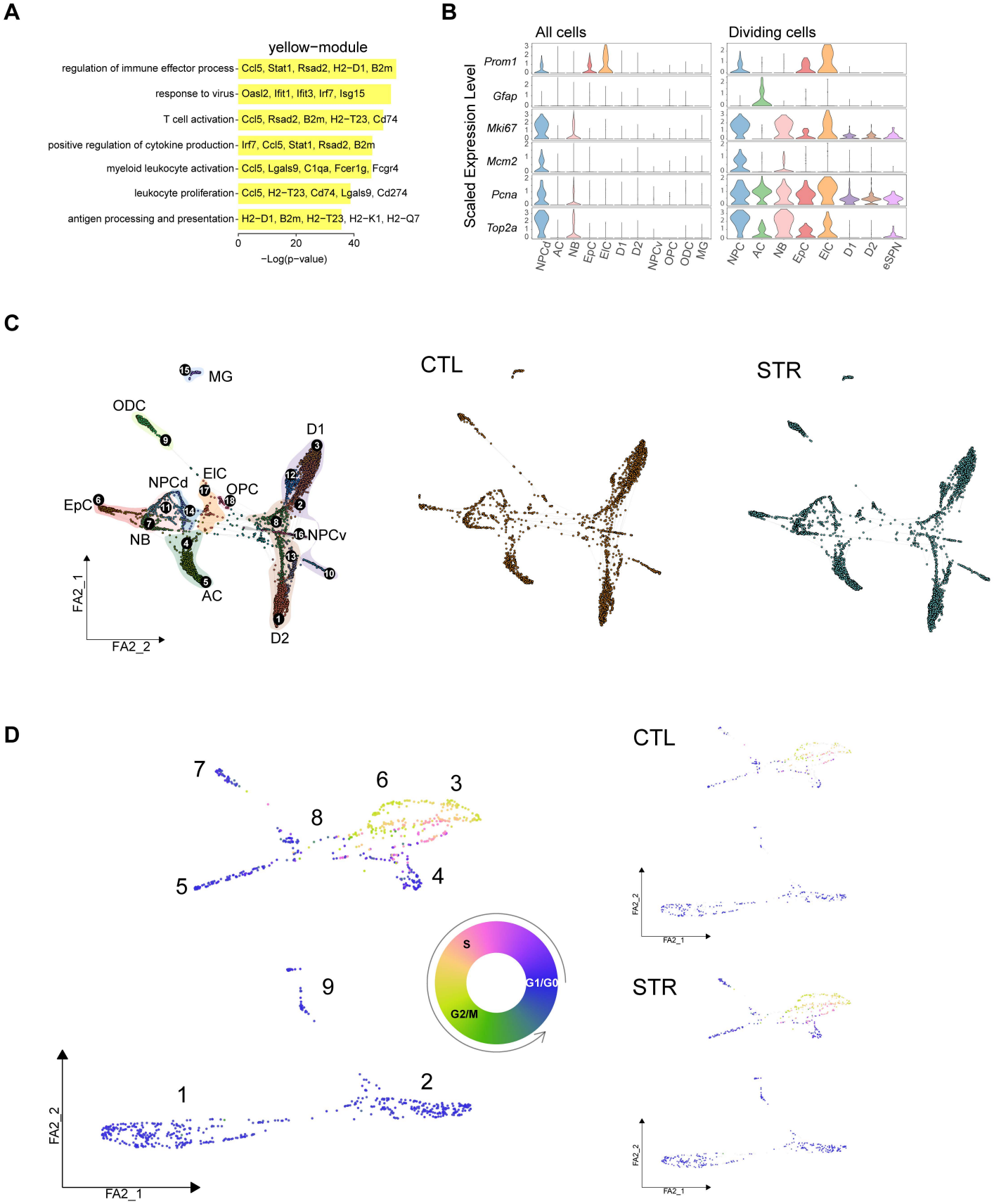
A
yellow−module
regulation of immune effector process- Ccl5, Stat1, Rsad2, H2−D1, B2m
response to virus- Oasl2, Ifit1, Ifit3, Irf7, Isg15
T cell activation- Ccl5, Rsad2, B2m, H2−T23, Cd74
positive regulation of cytokine production- Irf7, Ccl5, Stat1, Rsad2, B2m
myeloid leukocyte activation- Ccl5, Lgals9, C1qa, Fcer1g, Fcgr4
leukocyte proliferation- Ccl5, H2−T23, Cd74, Lgals9, Cd274
antigen processing and presentation- H2−D1, B2m, H2−T23, H2−K1, H2−Q7
0
20
40
−Log(p−value)
B
All cells
Dividing cells
Scaled Expression Level
Prom1
Gfap
Mki67
Mcm2
Pcna
Top2a
NPCd
AC
NB
EpC
EIC
D1
D2
NPCv
OPC
ODC
MG
NPC
eSPN
C
MG
ODC
D1
EIC
NPCd
OPC
EpC
NB
NPCv
AC
D2
FA2_1
FA2_2
CTL
STR
D
7
6
3
8
5
4
9
1
2
S
G1/G0
G2/M
FA2_1
FA2_2
CTL
STR

Sup. Figure 6

A

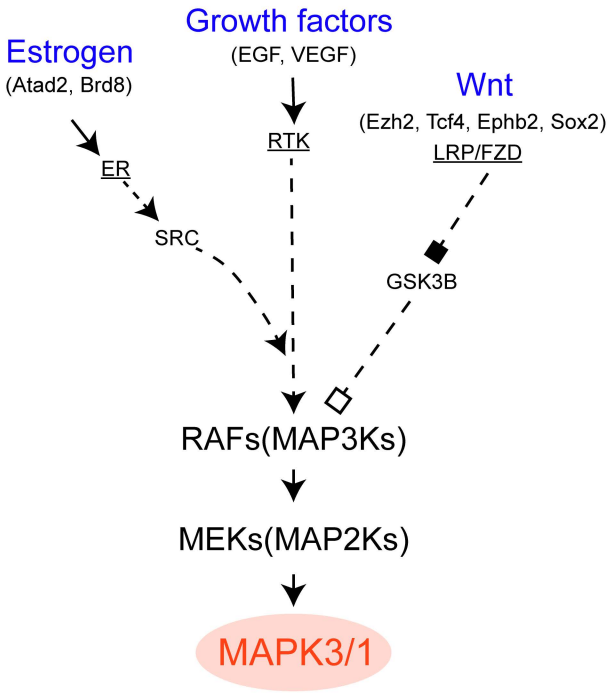

B

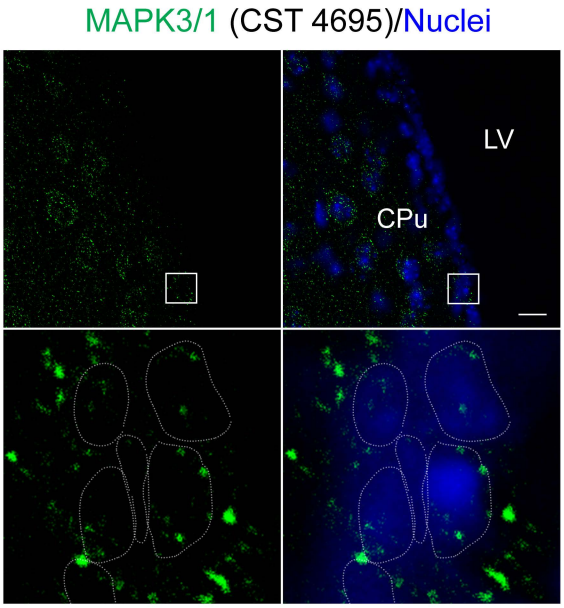

C

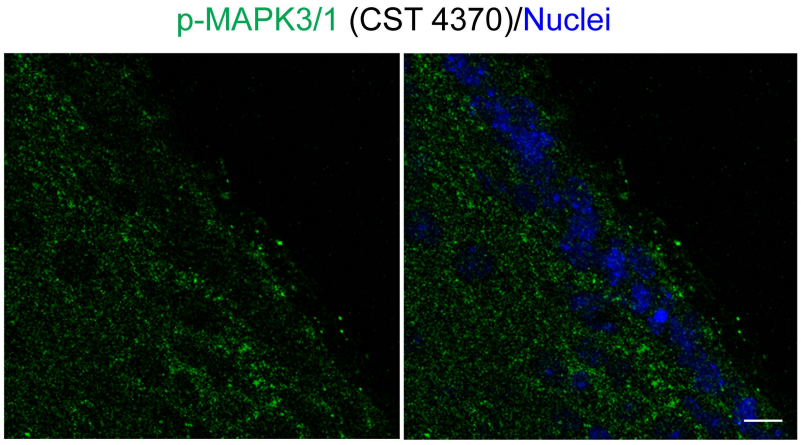

D

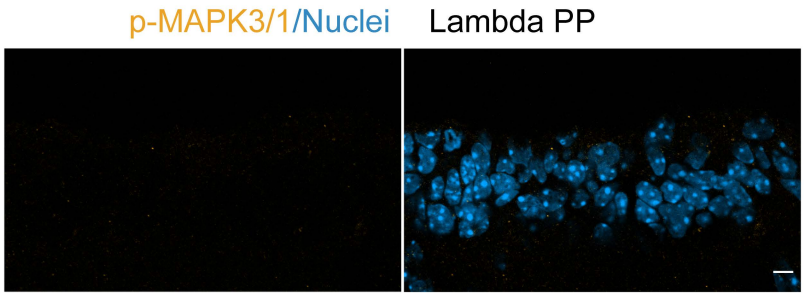

Sup. Table 1

Gene	GeneName	PAGErank_CTI	PAGErank_STF	Delta_PAGEra	Delta_PAGEra	avg_scaled_ex	avg_scaled_ex	alteration_STF
Grm5	glutamate rec	0.00296618	0.00642678	-0.0034606	4	0.1275909	-0.0747618	downregulate
Nfia	nuclear factor	0.00275617	0.00589953	-0.0031434	6	-0.1019362	0.05972942	upregulated
Tead1	TEA domain fa	0.00128305	0.00395694	-0.0026739	14	-0.1141115	0.06686351	upregulated
Zfp804a	zinc finger prc	0.00058589	0.00277351	-0.0021876	21	0.1184869	-0.0694273	downregulate
Ephb2	Eph receptor E	0.00140672	0.00346299	-0.0020563	24	-0.0948094	0.05555349	upregulated
Tia1	cytotoxic grar	0.00116659	0.00308805	-0.0019215	29	-0.0915264	0.05362984	upregulated
Ppargc1b	peroxisome pı	0.0023472	0.00424978	-0.0019026	30	0.10498992	-0.0615188	downregulate
Pou2f1	POU domain,	0.00129973	0.00311995	-0.0018202	31	-0.0813328	0.04765687	upregulated
Atad5	ATPase family,	0.00122132	0.00296819	-0.0017469	34	-0.1301323	0.0762509	upregulated
Slc8a2	solute carrier	0.00155996	0.00307168	-0.0015117	45	0.13042393	-0.0764218	downregulate
Zmiz1	zinc finger, MI	0.00103253	0.00252372	-0.0014912	48	-0.0652929	0.03825831	upregulated
Top2a	topoisomeras	0.00210639	0.00359632	-0.0014899	49	-0.0539777	0.03162819	upregulated
Ezh2	enhancer of ze	0.00091668	0.0024005	-0.0014838	51	-0.1004784	0.05887522	upregulated
Pde2a	phosphodiest	0.00149744	0.00296035	-0.0014629	52	0.09617283	-0.0563524	downregulate
Lin28b	lin-28 homolc	0.00176415	0.0031594	-0.0013952	56	0.06430435	-0.0376791	downregulate
Maml2	mastermind li	0.00177362	0.00316234	-0.0013887	57	-0.0854399	0.05006347	upregulated
Sox2	SRY (sex deter	0.00093969	0.00207047	-0.0011308	76	-0.0954706	0.05594093	upregulated
Trank1	tetratricopept	0.00059314	0.00163921	-0.0010461	88	0.14154706	-0.0829394	downregulate
Sox6	SRY (sex deter	0.00123881	0.00222725	-0.0009884	100	-0.1022588	0.05991847	upregulated
Zfpm2	zinc finger prc	0.00197797	0.00294047	-0.0009625	105	-0.1251619	0.07333851	upregulated
Foxn3	forkhead box I	0.00101353	0.00195636	-0.0009428	112	-0.1466464	0.08592736	upregulated
Zeb2	zinc finger E-b	0.00097512	0.0018519	-0.0008768	124	-0.0881966	0.05167872	upregulated
Gm11266	predicted gen	0.00107923	0.00189738	-0.0008182	139	-0.0716874	0.0420052	upregulated
Celf5	CUGBP, Elav-li	0.00203138	0.00280129	-0.0007699	151	0.16473163	-0.0965244	downregulate
Tcf4	transcription	0.00109495	0.0018191	-0.0007241	162	-0.1178551	0.06905713	upregulated
Mlip	muscular LMN	0.00116223	0.00181987	-0.0006576	179	0.10780983	-0.0631711	downregulate
Map4k4	mitogen-activ	0.00064407	0.00127925	-0.0006352	185	-0.1494163	0.08755037	upregulated
Mms22l	MMS22-like, D	0.00055588	0.0011265	-0.0005706	212	-0.087527	0.05128638	upregulated
Slit3	slit guidance l	0.00208095	0.00262969	-0.0005487	223	0.10541289	-0.0617666	downregulate
Arpp21	cyclic AMP-re	0.0007011	0.00121517	-0.0005141	237	0.19361576	-0.113449	downregulate
Atad2	ATPase family,	0.00303193	0.00346968	-0.0004377	297	-0.0635286	0.03722454	upregulated
Tox3	TOX high mob	0.00116927	0.00160485	-0.0004356	299	-0.0834976	0.04892533	upregulated
Nfib	nuclear factor	0.00137929	0.00178519	-0.0004059	323	-0.0543009	0.03181757	upregulated
Ncapg2	non-SMC conc	0.00070512	0.00109592	-0.0003908	338	-0.118198	0.06925804	upregulated
Ptprs	protein tyrosi	0.00050079	0.00089134	-0.0003905	339	-0.0985674	0.05775549	upregulated
Ryr3	ryanodine rec	0.00051285	0.00087241	-0.0003596	383	0.11271877	-0.0660475	downregulate
Ntrk3	neurotrophic	0.0023123	0.00266113	-0.0003488	398	0.12359809	-0.0724222	downregulate
Kcnd2	potassium vol	0.00078833	0.00110671	-0.0003184	434	0.12598583	-0.0738213	downregulate
Brip1os	BRCA1 interac	0.00059195	0.00089394	-0.000302	464	-0.1591957	0.09328057	upregulated
Sox5	SRY (sex deter	0.00170548	0.00200122	-0.0002957	471	-0.0893635	0.05236245	upregulated